Astronomy & Astrophysics

Infrared spectra of complex organic molecules in astronomically relevant ice matrices

I. Acetaldehyde, ethanol, and dimethyl ether

J. Terwisscha van Scheltinga[1,2,*], N. F. W. Ligterink[1,2,*], A. C. A. Boogert[3,4], E. F. van Dishoeck[2,5], and H. Linnartz[1]

[1] Raymond and Beverly Sackler Laboratory for Astrophysics, Leiden Observatory, Leiden University, PO Box 9513, 2300 RA Leiden, The Netherlands
    e-mail: [jeroentvs;linnartz]@strw.leidenuniv.nl
[2] Leiden Observatory, Leiden University, PO Box 9513, 2300 RA Leiden, The Netherlands
[3] Universities Space Research Association, Stratospheric Observatory for Infrared Astronomy, NASA Ames Research Center, Moffett Field, CA 94035, USA
[4] Institute for Astronomy, University of Hawaii, 2680 Woodlawn Dr., Honolulu, HI 98622, USA
[5] Max-Planck Institut für Extraterrestrische Physik (MPE), Giessenbackstr. 1, 85748 Garching, Germany

ABSTRACT

Context. The number of identified complex organic molecules (COMs) in inter- and circumstellar gas-phase environments is steadily increasing. Recent laboratory studies show that many such species form on icy dust grains. At present only smaller molecular species have been directly identified in space in the solid state. Accurate spectroscopic laboratory data of frozen COMs, embedded in ice matrices containing ingredients related to their formation scheme, are still largely lacking.

Aims. This work provides infrared reference spectra of acetaldehyde (CH_3CHO), ethanol (CH_3CH_2OH), and dimethyl ether (CH_3OCH_3) recorded in a variety of ice environments and for astronomically relevant temperatures, as needed to guide or interpret astronomical observations, specifically for upcoming *James Webb* Space Telescope observations.

Methods. Fourier transform transmission spectroscopy (500–4000 cm^{-1}/20–2.5 µm, 1.0 cm^{-1} resolution) was used to investigate solid acetaldehyde, ethanol and dimethyl ether, pure or mixed with water, CO, methanol, or CO:methanol. These species were deposited on a cryogenically cooled infrared transmissive window at 15 K. A heating ramp was applied, during which IR spectra were recorded until all ice constituents were thermally desorbed.

Results. We present a large number of reference spectra that can be compared with astronomical data. Accurate band positions and band widths are provided for the studied ice mixtures and temperatures. Special efforts have been put into those bands of each molecule that are best suited for identification. For acetaldehyde the 7.427 and 5.803 µm bands are recommended, for ethanol the 11.36 and 7.240 µm bands are good candidates, and for dimethyl ether bands at 9.141 and 8.011 µm can be used. All spectra are publicly available in the Leiden Database for Ice.

Key words. astrochemistry – methods: laboratory: molecular – techniques: spectroscopic – molecular processes

1. Introduction

Water was the first molecule to be detected in the solid state in the interstellar medium (Gillett & Forrest 1973). Since then more than 10 other molecules have been identified in icy form (i.e. CO, CO_2, CH_4, NH_3 and CH_3OH) and it has become clear that icy dust grains play a key role in the formation of both these small molecules and more complex organic molecules (COMs), such as glycolaldehyde ($HOCH_2CHO$) and ethylene glycol ($HOCH_2CH_2OH$). The combined outcome of astronomical observations, specifically space based missions such as the Infrared Space Observatory (ISO) and *Spitzer* Space Telescope (Kessler et al. 1996; Werner et al. 2004), laboratory, and astrochemical modelling studies have resulted in a detailed picture of the composition and structure of ice mantles on interstellar dust grains and the chemical processes taking place (see reviews by Gibb et al. 2000; Herbst & van Dishoeck 2009; Öberg et al. 2011;

Caselli & Ceccarelli 2012; Tielens 2013; Boogert et al. 2015; Linnartz et al. 2015; Öberg 2016). It is generally accepted that interstellar ices form on the surface of dust grains in cold dark clouds through accretion in two distinct layers: a polar H_2O-rich and an apolar CO-rich layer. Water, together with NH_3, CO_2, and CH_4, forms through atom addition reactions in lower density environments (Hiraoka et al. 1995; Miyauchi et al. 2008; Oba et al. 2009,2012; Dulieu et al. 2010; Hidaka et al. 2011; Linnartz et al. 2011; Lamberts et al. 2013, 2014; Fedoseev et al. 2015). At later stages, when densities increase and temperatures decrease along with the ongoing cloud collapse, CO freeze-out from the gas phase occurs, forming a CO coating on top of the water rich layer (Tielens et al. 1991; Pontoppidan 2006). Subsequent hydrogenation processes transform CO to H_2CO and H_2CO to CH_3OH (Watanabe & Kouchi 2002; Fuchs et al. 2009), resulting in CO ice intimately mixed with methanol (Cuppen et al. 2011; Penteado et al. 2015). Radical recombination processes in various starting mixtures, triggered by energetic (i.e. UV photons or
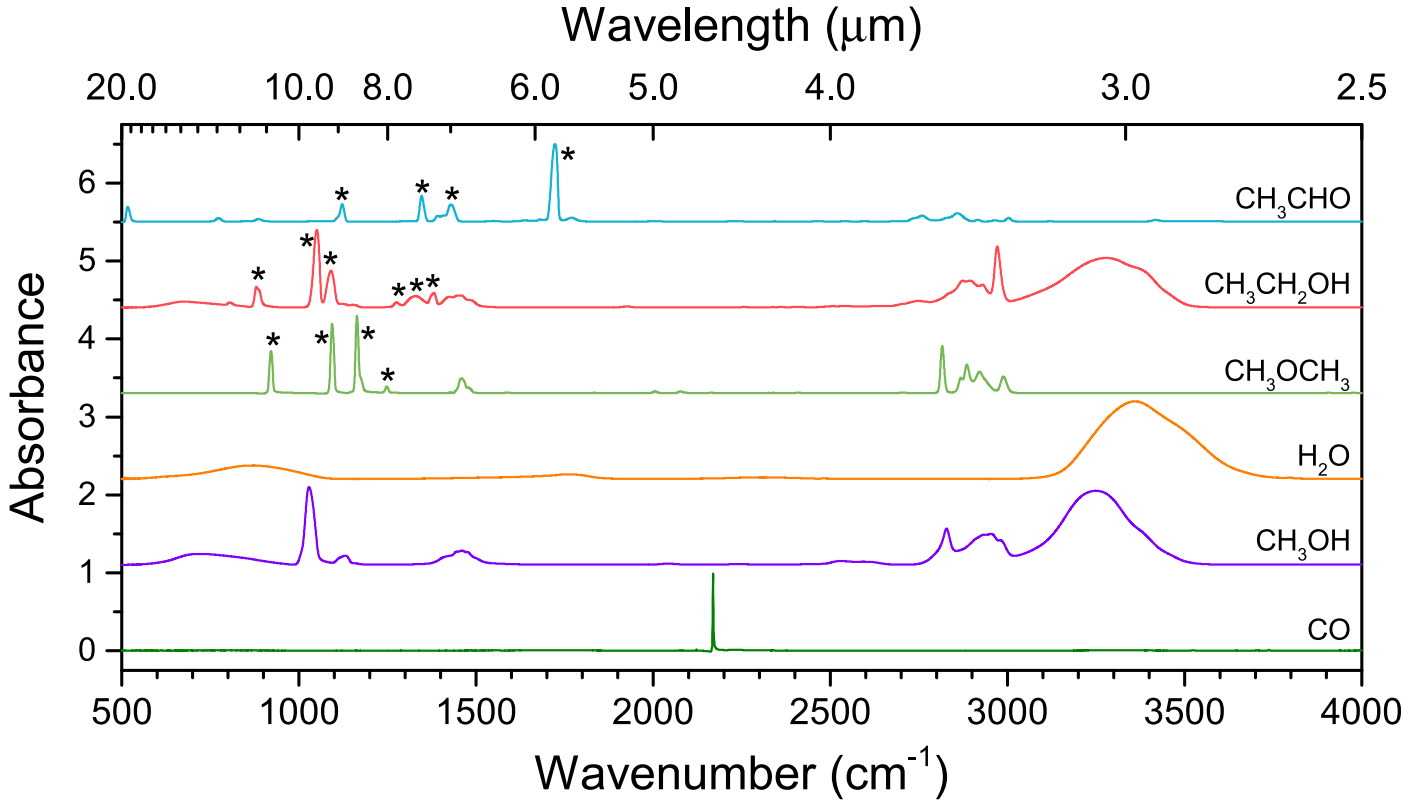

Fig. 1. Spectra of pure acetaldehyde (blue), ethanol (red), dimethyl ether (green), water (orange) methanol (purple), and CO (dark green) normalized to one in the range of 2.5–20.0 μm. The bands investigated in this work are indicated with an asterisk (*).
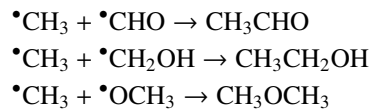
cosmic rays) or non-energetic (i.e. atom additions) were shown to provide pathways towards the formation of more complex molecules (see reviews of Linnartz et al. 2015; Öberg 2016).

The molecules H_2O, CO, CO_2, CH_4, NH_3, and CH_3OH make up the bulk of interstellar ice (Ehrenfreund & Charnley 2000; Öberg et al. 2011), but less abundant species have been observed as well. These include species such as OCS and OCN^- (Palumbo et al. 1995; van Broekhuizen et al. 2004). A number of COMs, such as formic acid (HCOOH), acetaldehyde (CH_3CHO), and ethanol (CH_3CH_2OH), have been tentatively detected based on spectroscopic features at 7.2 and 7.4 μm (Schutte et al. 1999; Öberg et al. 2011). Several other spectroscopic features, such as the 6.0 and 6.8 μm bands, remain only partly identified (Schutte et al. 1996; Boudin et al. 1998; Gibb & Whittet 2002; Boogert et al. 2008). Limited astronomical detection sensitivity combined with a lack of high resolution laboratory data have thus far prohibited secure solid state identifications of COMs other than methanol, but their presence in interstellar ices is generally accepted and also further supported by the recent detection of a number of COMs on comet 67P/Churyumov–Gerasimenko and in its coma (Goesmann et al. 2015; Altwegg et al. 2017).

With the upcoming launch of the *James Webb* Space Telescope (JWST) in 2019, new instruments such as MIRI (Mid InfraRed Instrument; Wright et al. 2015) and NIRSpec (Near InfraRed Spectrograph; Posselt et al. 2004) will become available to record telluric free spectra of interstellar ices at higher spectral and spatial resolution and with higher sensitivity than possible so far. This opens up new possibilities to search for and study the level of molecular complexity in interstellar ices. To aid in the search for larger molecules in the solid state, high resolution IR laboratory spectra are required. The ice matrix environment and its temperature have to be taken into account

since these influence the spectral appearance of vibrational bands.

In this work we present the infrared spectra of acetaldehyde, ethanol, and dimethyl ether, respectively, CH_3CHO, CH_3CH_2OH, and CH_3OCH_3. The choice for these three species, an aldehyde, an alcohol, and an ether, is motivated by previous tentative identifications (Boudin et al. 1998; Schutte et al. 1999; Öberg et al. 2011), their astronomical gas-phase identification and high abundance (e.g. Turner 1991; Gibb et al. 2000; Cazaux et al. 2003; Bisschop et al. 2007b; Taquet et al. 2015; Müller et al. 2016), and their common formation scheme upon UV irradiation of methanol ice (Öberg et al. 2009). Formation of these molecules is seen in energetic processing experiments of methanol ice (Gerakines et al. 1996; Bennett et al. 2007; Öberg et al. 2009; Boamah et al. 2014) and starts with cleavage of the CH_3OH bonds. This results in a reservoir of radicals that can be used for their formation as follows:

$$^\bullet CH_3 + {}^\bullet CHO \rightarrow CH_3CHO$$

$$^\bullet CH_3 + {}^\bullet CH_2OH \rightarrow CH_3CH_2OH$$

$$^\bullet CH_3 + {}^\bullet OCH_3 \rightarrow CH_3OCH_3$$

Formation of dimethyl ether and ethanol has also been studied by radical recombination reactions starting from CH_4:H_2O mixtures (Bergantini et al. 2017). Besides energetic radical recombination reactions, other formation pathways and links between the three molecules exist as well. For example, acetaldehyde has been proposed as a solid state precursor of ethanol. A hydrogen atom addition experiment showed that acetaldehyde can at least partially (>20%) be transformed into ethanol (Bisschop et al. 2007a). Acetaldehyde itself has been proposed to form as a spin-off in the well-studied

$CO + H \rightarrow HCO \rightarrow H_2CO \rightarrow H_3CO \rightarrow CH_3OH$ chain (Charnley 2004); HCO may directly interact with a C-atom, to form HCCO that upon hydrogenation yields CH_3CHO (Charnley & Rodgers 2005).

This work presents a detailed study of the IR spectral characteristics of CH_3CHO, CH_3CH_2OH, and CH_3OCH_3 in pure form and mixed in the interstellar relevant ice matrices H_2O, CO, CH_3OH, and $CO:CH_3OH$. Section 2 contains the experimental details and measurement protocols. The results of the measurements are presented and discussed in Sect. 3. In Sect. 4 the astronomical relevance of the new data is illustrated. The conclusions are summarized in Sect. 5. A complete overview with all data obtained in this study is available from the appendices.

2. Experimental

2.1. Set-up

The ice spectra are recorded in a high-vacuum (HV) set-up, which is described in detail by Bossa et al. (2015). A central stainless steel chamber is evacuated by a $300\,l\,s^{-1}$ turbomolecular pump, backed by a double stage rotary vane pump ($8\,m^3\,h^{-1}$). This allows a base pressure of $\sim 10^{-7}$ mbar at room temperature. The pressure is monitored by an Agilent FRG-720 full range gauge. Ices are grown on an infrared transmissive ZnSe window that is cryogenically cooled to a lowest temperature of $12\,K$ by a closed cycle helium cryostat. The temperature of the window is monitored by a LakeShore 330 temperature controller, which regulates a feedback loop between a resistive heating wire and a silicon diode temperature sensor. An absolute temperature accuracy of $\pm 2\,K$ and a relative accuracy of $\pm 1\,K$ is acquired with this diode. The IR beam of a Fourier Transform InfraRed Spectrometer (FTIRS; Varian 670-IR) is aligned through the window to obtain IR spectra of the samples. The spectrometer covers a range of $4000\text{–}500\,cm^{-1}$ ($2.5\text{–}20\,\mu m$) at spectral resolutions as high as $0.1\,cm^{-1}$. Samples are externally prepared in a 2L glass bulb using a separate multi-line gas mixing system. The gas mixing line is turbomolecularly pumped to pressures $<1 \times 10^{-4}$ mbar. Gas mixtures are made by sequential addition of its components. Two gas independent gauges, covering various pressure ranges ensure that accurate mixing ratios are obtained with a maximum error of $<10\%$. The liquids and gases used in these experiments are acetaldehyde (Sigma–Aldrich, 99.5%), ethanol (Biosolve, 99.9%), dimethyl ether (Sigma–Aldrich, 99.9%), water (Milli-Q, Type I), carbon monoxide (Linde gas, 99.997%), and methanol (Sigma–Aldrich, 99.9%). Liquid samples are purified with freeze-pump-thaw cycles before use.

2.2. Measurement protocol

Pure or premixed gases are background deposited onto the 15 K cold sample via an inlet valve. A standard pressure of 20 mbar in the glass bulb is used to prevent a decreasing inlet pressure gradient during deposition. Bi-mixed gases are prepared in a 1:20 ratio and tri-mixed gases in a 1:20:20 ratio, where the smallest fraction is the COM under investigation. These dilution factors ensure that the COM mainly interacts with the surrounding matrix, resulting in matrix shifted IR vibrational bands. Ices are grown at 15 K to a column density of $\sim 4500\,ML$ (1 monolayer is $1 \times 10^{15}\,mol\,cm^{-2}$) on the window. This coverage ensures that any influence of background contamination, mainly water depositing at a rate of less than $30\,ML\,h^{-1}$, can be neglected. During deposition, IR spectra are recorded at $1\,cm^{-1}$ resolution

($0.5\,cm^{-1}$ step size) and averaged over 61 scans (equals 2 min) to trace the ice growth and determine when the ice is $\sim 4500\,ML$ thick. From the integration of the IR band absorption, the column density of the species $N_{species}$ is determined according to

$$N_{species} = \ln(10)\frac{\int_{band} \log_{10}\left(\frac{I_0(\tilde{\nu})}{I(\tilde{\nu})}\right) d\tilde{\nu}}{A'}, \tag{1}$$

where $\int_{band} \log_{10}\left(\frac{I_0(\tilde{\nu})}{I(\tilde{\nu})}\right) d\tilde{\nu}$ is the integrated absorbance of the band and $I_0(\tilde{\nu})$ and $I(\tilde{\nu})$ are the flux received and transmitted by the sample, respectively, and A' is the apparent band strength in $cm\,mol^{-1}$. It is important to realize that strongly absorbing bands may get saturated at high coverages, resulting in unreliable column density measurements. In the experiments conducted, the CO band at $2135\,cm^{-1}$ reaches saturation at high coverage, as do certain bands of pure acetaldehyde and dimethyl ether. For these species, bands with a lower band strength or isotopologues can be used. The measured column densities give an indication whether the mixed ice composition still matches the gas-phase mixing ratio and whether the COMs are sufficiently diluted in the matrix. Small variations in the composition of the gas mixture and matrix interactions complicate accurate ice mixing ratio determinations. The apparent band strengths are listed in Table 1 and taken from literature for acetaldehyde and ethanol. For the dimethyl ether bands at 923, 1095, and $1164\,cm^{-1}$ the band strength value is approximated from a methane:dimethyl ether mixture, prepared at a one to one ratio in the gas phase. Assuming this ratio is maintained in the ice and matrix interactions are negligible, the apparent band strength is determined from a comparison with the methane $1302\,cm^{-1}$ band area and its known apparent band strength of $8.0 \times 10^{-18}\,cm\,mol^{-1}$ (Bouilloud et al. 2015).
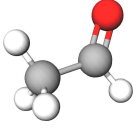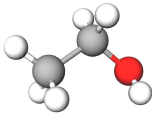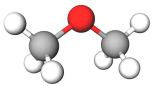
After deposition the sample is linearly heated at a rate of $25\,K\,h^{-1}$, until it is fully desorbed from the window. The low temperature ramp ensures that the ice has sufficient time to undergo structural changes, particularly from the amorphous to the crystalline phase. During heating IR spectra are continuously recorded and averaged over 256 scans to trace spectral changes vs. temperature.

2.3. Analysis protocol

Owing to the very large amount of spectra that are recorded during the experiments, we only present samples of representative IR spectra for temperatures at which significant spectral changes occur. These spectra are baseline subtracted and the peak position and band width at full width at half maximum (FWHM) are determined for selected spectral features. When the band of a COM overlaps with a spectral feature of a matrix molecule, also the matrix feature is subtracted where possible. In the case of band splitting, the least intense component is only taken into account when its peak position is clearly distinguishable. In a few cases splitted peaks rival in intensity and are heavily overlapping and it is not possible to fit a FWHM for the individual components. Here the FWHM of the combined peaks is determined. Peaks are selected for analysis mainly based on their intensity and potential as an ice tracer, i.e. selecting wavelengths for which no strong overlap with known interstellar features exist.

Identification of vibrational modes of the three species studied here is realized by comparison with available spectra from liquid and solid state literature (Plyler 1952; Evans & Bernstein 1956; Barnes & Hallam 1970; Allan et al. 1971;

Table 1. Selected bands of acetaldehyde, ethanol, and dimethyl ether.

| Species | Formula | Mode | Peak position* | | A' |
			cm^{-1}	μm	cm mol^{-1}
Acetaldehyde	CH_3CHO	CH_3 rock. + CC stretch. + CCO bend.	1122.3	8.909	
		CH_3 s-deform. + CH wag.	1346.2	7.427	
		CH_3 deform.	1429.4	6.995	
		CO stretch.	1723.0	5.803	$1.3 \times 10^{-17\,a}$
Ethanol	CH_3CH_2OH	CC stretch.	879.8	11.36	$3.24 \times 10^{-18\,b}$
		CO stretch.	1051.0	9.514	$1.41 \times 10^{-17\,b}$
		CH_3 rock.	1090.5	9.170	$7.35 \times 10^{-18\,b}$
		CH_2 tors.	1275.2	7.842	
		OH deform.	1330.2	7.518	
		CH_3 s-deform.	1381.3	7.240	
Dimethyl ether	CH_3OCH_3	COC stretch.	921.3	10.85	$5.0 \times 10^{-18\,c}$
		COC stretch. + CH_3 rock.	1093.9	9.141	$9.2 \times 10^{-18\,c}$
		COC stretch. + CH_3 rock.	1163.8	8.592	$9.8 \times 10^{-18\,c}$
		CH_3 rock.	1248.2	8.011	

Notes. [*] Peak position of the pure molecule at 15 K. Note that throughout literature there seems to be disagreement in the assignment of certain modes, particularly for ethanol.
References. [a] Schutte et al. (1999). [b] Hudson (2017). [c] This work.

Hollenstein & Günthard 1971; Mikawa et al. 1971; Coussan et al. 1998). Optical effects such as longitudinal optical–transverse optical (LO-TO) splitting and particle shape effects are not explicitly taken into account. Since spectra are recorded at normal incidence with unpolarized light, only the TO modes are recorded. However, certain combinations of polarized light and angles of incidence can result in the LO phonon mode showing up (Baratta et al. 2000; Palumbo et al. 2006). Also particle shape effects can shift transition bands with respect to recorded laboratory spectra (Baratta & Palumbo 1998). Such effects affect only the spectra of more abundant species, such as CO or CO_2, and are not considered to be relevant for COMs.

3. Results and discussion

In this section selected results of the acetaldehyde, ethanol, and dimethyl ether experiments are presented. These are representative for the much larger data set given in the appendix. All the selected spectra used in this work are publicly available from the Leiden Database for Ice[1], spectra recorded for other temperatures are available on request. Figure 1 shows the IR spectra of pure acetaldehyde, ethanol, and dimethyl ether ice at 15 K; the bands that are fully analysed are indicated with an asterisk (*) and spectra of pure water, CO, and methanol ice. Figures of the spectra of COMs mixed in water, CO, methanol, and CO:methanol at 15 K are shown in Appendix A. In Table 1, these selected bands are listed together with their peak positions and, if available, apparent band strength in pure ices at 15 K. Appendix B presents the results of the analysis of the selected bands, listing peak positions, FWHMs, and

integrated absorbance ratios at various temperatures and for different ice matrices. A representative example of the tables listed in the appendix is shown in Table 2 for the acetaldehyde CH_3 s-deformation + CH wagging mode at 1346.6 cm^{-1} at 15 K.

For easier interpretation the results are represented in a number of plots; see Figs. 2–4 for examples. Each plot covers the data of one band. In all plots, the top panels show spectroscopic changes of the band under thermal processing in pure and mixed ices. The bottom left panels plot peak position vs. FWHM, showing trends in the band. The bottom right panels give an indication of how the band strengths change relative to each other in various matrices. Assuming that the ice column density is roughly the same for each experiment and that the gas mixing ratio is close to the ice mixing ratio, the mixed ices are corrected for their dilution factor. Owing to various uncertainties in this method, this results in relatively large error bars for the band strengths. This is unfortunate as this would allow us to interpret the spectroscopic identifications – the primary goal of this work – also in terms of accurate column densities. The remaining figures of other bands can be found in Appendix C.

A few general statements can be made. Most peaks display peak narrowing under thermal processing, which is due to the ice changing to a crystalline phase with increasing temperature. Mixed ice in CO and CO:CH_3OH are exceptions due to the volatility of CO and its removal from the ice at relatively low temperatures. Above 30 K, the desorption temperature of CO (Öberg et al. 2005), these ices are often seen to display peak broadening.

Peak splitting, especially at high temperatures is another effect that is generally seen. This can be caused by two or more modes contributing to a single feature at low temperatures and becoming visible as the peaks begin to narrow at higher temperatures. Alternatively, the matrix can play a role and a peak is

---

[1] http://icedb.strw.leidenuniv.nl

Fig. 2. *Top*: *from left to right* the acetaldehyde 7.427 μm band pure (black) and in water (red), CO (blue), methanol (purple), and CO:CH$_3$OH (green) at various temperatures. *Bottom left*: peak position vs. FWHM plot, using the same colour coding. *Bottom right*: the relative band strength for the 7.427 μm band at 15 K in various matrices.

split owing to different interactions of a functional group with its surroundings. For example, an ice can segregate under thermal processing and have part of the COM still intimately mixed with the matrix molecule, while another part is forming COM clusters. Segregation is an effect most clearly seen in the COM:CO ice mixtures.

Integrated absorbance ratios are given for the bands under investigation in each ice mixture. These ratios can provide a tool to estimate the likelihood of observing other bands upon detection of a specific transition. They can also be used as conversion factors to determine band strengths from known band strengths.

The bands are normalized on the band with highest integrated absorbance at 15 K, unless this band is suspected to be in saturation or when the data set is incomplete over the investigated temperature range.

3.1. Acetaldehyde

Acetaldehyde hosts four significant features in the 5.5–12.5 μm region (see Fig. 1). Some smaller features are also visible, such as the CC stretching + CH$_3$ rocking mode close to 11 μm, however, its intensity is very small compared to the other bands. Two

Table 2. Peak position and FWHM of the acetaldehyde CH_3 s-deformation + CH wagging mode at 15 K in various matrices.

Mixture	Temperature (K)	$\lambda_{peak,-baseline}$		$\lambda_{peak,-matrix}$		FWHM	
		(cm^{-1})	(μm)	(cm^{-1})	(μm)	(cm^{-1})	(μm)
CH_3CHO		1346.6	7.4264	–	–	13.5	0.0744*
$CH_3CHO:H_2O$		1349.9	7.4078	1349.9	7.4078	9.2	0.0502
$CH_3CHO:CO$	15	1349.4	7.4104	–	–	4.8	0.0262
$CH_3CHO:CH_3OH$		1347.5	7.4211	–	–	13.0	0.0714
$CH_3CHO:CO:CH_3OH$		1349.4	7.4105	–	–	12.6	0.0691

Notes. Excerpt from Table B.1. $^{(*)}$ FWHM result of two or more blended peaks.

characteristic vibrational modes of acetaldehyde at 6.995 and 8.909 μm coincide with methanol CH_3 rocking and deformation modes and are likely obscured in interstellar spectra. A solid state identification of acetaldehyde based on these vibrational modes is unlikely. The CO stretching mode is the most prominent band in this spectrum. However, its location at 5.8 μm coincides with the CO stretching mode of many other molecules, such as formaldehyde (H_2CO), formic acid (HCOOH), or formamide (NH_2CHO), which are expected to be present in interstellar ice, making it likely that this band is blended. The fourth band is the CH_3 s-deformation + CH wagging mode around 7.427 μm, which is found to have no substantial overlap with abundant bulk interstellar ice components and therefore is most suited for a successful solid state identification of this molecule.

Figure 2 shows the results of the analysed data of the CH_3 s-deformation + CH wagging band. Under thermal processing the band widths are generally seen to decrease; this is caused by crystallization in the ice. Peak positions shift as well, with clear blue shifting trends visible for the $CO:CH_3OH$ and water mixtures. In the case of the $CO:CH_3OH$ mixture this is likely because of the loss of CO from the matrix, while for the water mixture the interaction between acetaldehyde and crystalline water is more likely the cause. In some cases, at high temperature CH_3CHO undergoes peak splitting, making identification through FWHM challenging. However, this can also be used as a tool to determine the ice temperature. The comparison of peak position makes it in general easy to distinguish between pure acetaldehyde, acetaldehyde mixed in CH_3OH, and $CO:CH_3OH$, acetaldehyde mixed in CO, and acetaldehyde mixed in water. The 7.427 μm band shows a substantial decrease in band strength by about 40% when acetaldehyde is surrounded by matrix molecules.

The acetaldehyde CO stretching band underlines the above findings, given it is clearly observed (see Fig. C.3). Especially at low ice temperatures of 15 and 30 K clear peak shifts are visible between the $CO:CH_3OH$ matrix at 5.84 μm, the water matrix at 5.825 μm, and the pure matrix, or in a CH_3OH matrix at around 5.805 μm.

3.2. Ethanol

The spectrum of pure ethanol in Fig. 1 shows a strong CC stretching band at 11.36 μm, CO stretching mode at 9.514 μm, and CH_3 rocking mode at 9.170 μm. A number of weaker modes are seen between 6.5 and 8.5 μm: specifically the CH_2 torsion mode at 7.842 μm, the OH deformation mode at 7.518 μm, and the CH_3 symmetric deformation mode at 7.240 μm. Overlap with spectral features of bulk interstellar ice species such as water and methanol is an issue for the three strongest bands, coinciding with either the water libration mode or CO stretching and CH_3 rocking modes of methanol. Also the prominent broad silicate

feature is present at ~9.7 μm. Although the other ethanol modes are substantially weaker, they fall within a spectral region that is generally clean of strong transitions.

The ethanol 7.240 μm band is a possible candidate for identification. Figure 3 shows the data of this band. Ethanol mixed in water can be distinguished from other features by a ~3 cm^{-1} peak shift from other mixtures. In general it is found that the ethanol:water mixture is relatively easy to distinguish, but the other mixtures display much overlap in peak position and FWHM. The CH_2 torsion, OH deformation mode, and CH_3 symmetric deformation mode are hard to identify in the ethanol:CO mixture owing to the appearance of many more modes. Band areas and relative band strengths of these modes are therefore not considered. The band strength is seen to vary substantially for the various bands, but does not show a clear trend.

3.3. Dimethyl ether

Three strong bands of dimethyl ether are found at 10.85, 9.141, and 8.592 μm for the COC stretching and two COC stretching + CH_3 rocking modes, respectively. A much weaker CH_3 rocking mode is found at 8.011 μm. The first two overlap with known interstellar ice features of methanol, water, and silicates and are therefore less suited for an identification, while the third likely falls in the wing of such features and may still be used. Even though it is a weak mode, the 8.011 μm band falls in a relatively empty region of interstellar ice spectra. This feature could therefore be most suited for a dimethyl ether identification; see Fig. 4.

For the 8.011 μm band clear differences are seen depending on the matrix. The spectra of pure and methanol mixture are distinguishable from those of the water and $CO:CH_3OH$ mixtures by a ~2 cm^{-1} peak shift of the low temperature spectra at 15 and 30 K. In water this band displays a narrower peak compared to the other ices. The other bands also show many clear differences in peak position and FWHM between the various ice mixtures. A characteristic peak splitting structure at low temperatures is seen for the 10.85 μm band when mixed in water, methanol, or $CO:CH_3OH$. Interestingly, the relative band strength shows a substantial increase in the CH_3OH and $CO:CH_3OH$ mixtures for the 8.011 μm band. Other modes do not show such clear differences. Also it is interesting to note the fact that the COC stretching mode has the largest band area when mixed in water, while in the other mixtures this is always the CH_3 rocking mode at 8.592 μm (see Appendix B.6).

4. COM ice features in W33A

Our extensive measurements of frozen COMs are needed in the analysis of the many spectra of dense clouds, embedded
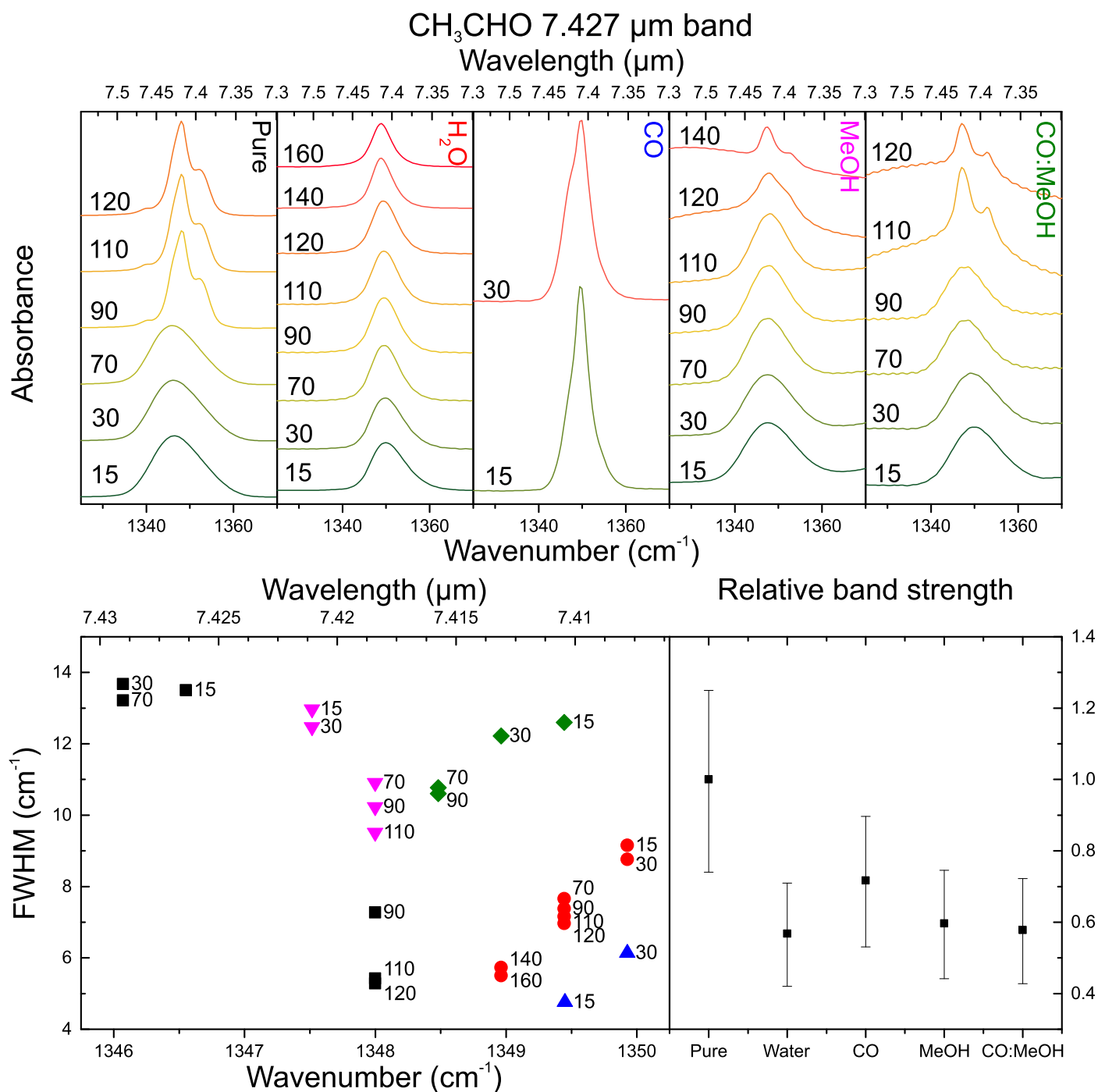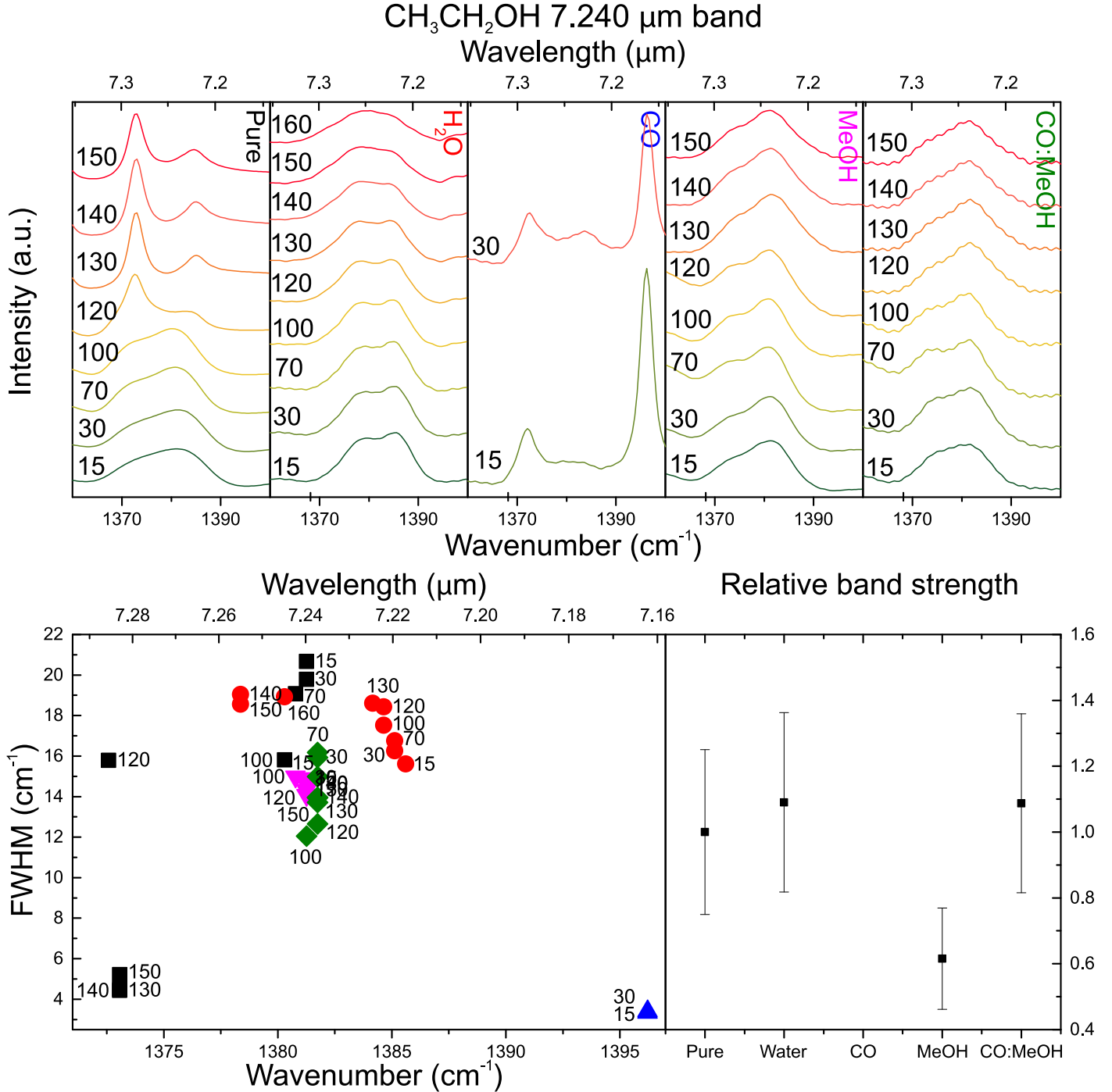
Fig. 3. *Top*: *from left to right* the ethanol 7.240 μm band pure (black) and in water (red), CO (blue), methanol (purple), and CO:CH$_3$OH (green) at various temperatures. *Bottom left*: peak position vs. FWHM plot, using the same colour coding. *Bottom right*: the relative band strength for the 7.240 μm band at 15 K in various matrices.

protostars, and inclined protoplanetary disks that will be obtained with the upcoming *JWST* mission at high sensitivity and medium spectral resolution (R of up to 3500). Here, we demonstrate their use by a reanalysis of a spectrum of the massive protostar W33A obtained with the Infrared Space Observatory's Short Wavelength Spectrometer (Astronomical Observation Template 1; $R = 800$). This is one of the few sources for which a high quality mid-IR spectrum is available (Gibb et al. 2000). In the 7 to 8 μm region three prominent features at 7.25, 7.41, and 7.67 μm have been described previously in

the literature. The 7.25 μm feature has been attributed to both CH$_3$CH$_2$OH and HCOOH (Schutte et al. 1999; Öberg et al. 2011), the 7.41 μm feature has been attributed to HCOO$^-$ and CH$_3$CHO (Schutte et al. 1999), and the 7.67 μm band has been identified as solid methane with potentially contributions of SO$_2$ (Boogert et al. 1996).

In this work we make use of the water and silicate subtracted spectrum of W33A, shown in Fig. 5 with a straight line local continuum subtraction. The aforementioned features are visible, although the 7.41 μm feature seems to have two contributions at
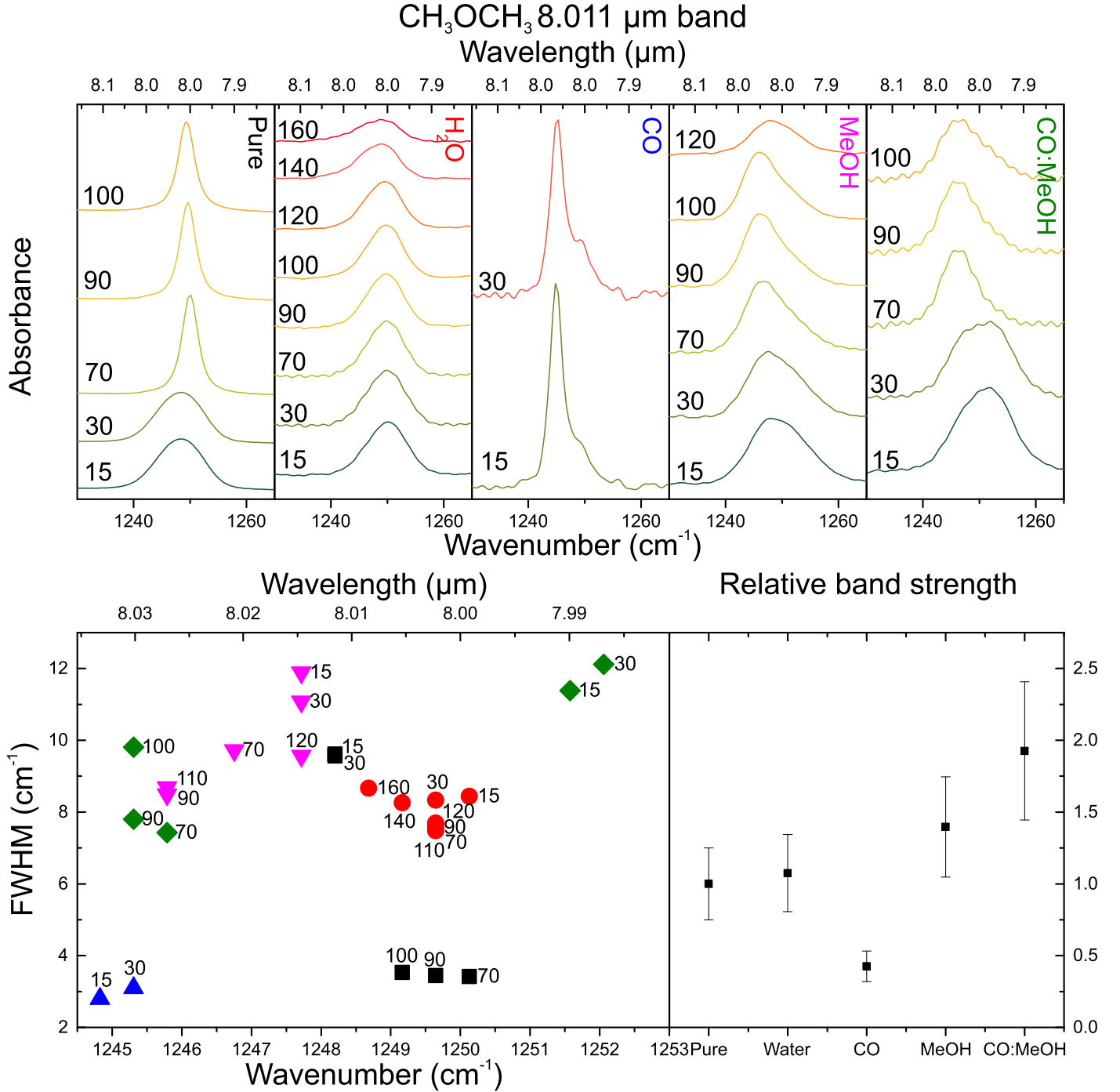
Fig. 4. *Top: from left to right* the dimethyl ether 8.011 μm band pure (black) and in water (red), CO (blue), methanol (purple), and CO:CH$_3$OH (green) at various temperatures. *Bottom left*: peak position vs. FWHM plot, using the same colour coding. *Bottom right*: the relative band strength for the 8.011 μm band at 15 K in various matrices.

7.47 and 7.40 μm and the 7.25 μm feature is found at 7.22 μm. The spectra of ethanol and acetaldehyde mixed in CO:CH$_3$OH and H$_2$O are plotted in the same figure. The peak position of the 7.40 μm feature can be reproduced well by the acetaldehyde CH$_3$ s-deformation mode in both mixtures. However, the band in CO:methanol mixture seems to be too broad to justly reproduce the W33A 7.40 μm feature and also this band covers the 7.47 μm feature next to it. The other two features at 7.22 and 7.47 μm could be the result of the CH$_3$ s-deformation and OH deformation modes of ethanol. Particularly, the CH$_3$CH$_2$OH:H$_2$O mixture coincides with the peak locations of the 7.22 and 7.47 μm

features in the W33A spectrum. While the identification of acetaldehyde and ethanol are plausible, detection of additional features would strengthen the assignment. We checked and found that none of the other CH$_3$CHO and CH$_3$CH$_2$OH bands have an anti-coincidence with the W33A spectrum.

Upper limits to the ice column densities of ethanol and acetaldehyde can be given based on the integrated optical depth of their potential features. Schutte et al. (1999) give integrated τ values of 2.0 ± 0.3 and 1.6 ± 0.5 cm^{-1}, respectively. Band strength values of ethanol and acetaldehyde are taken from the literature and used to calculate the column densities of the two
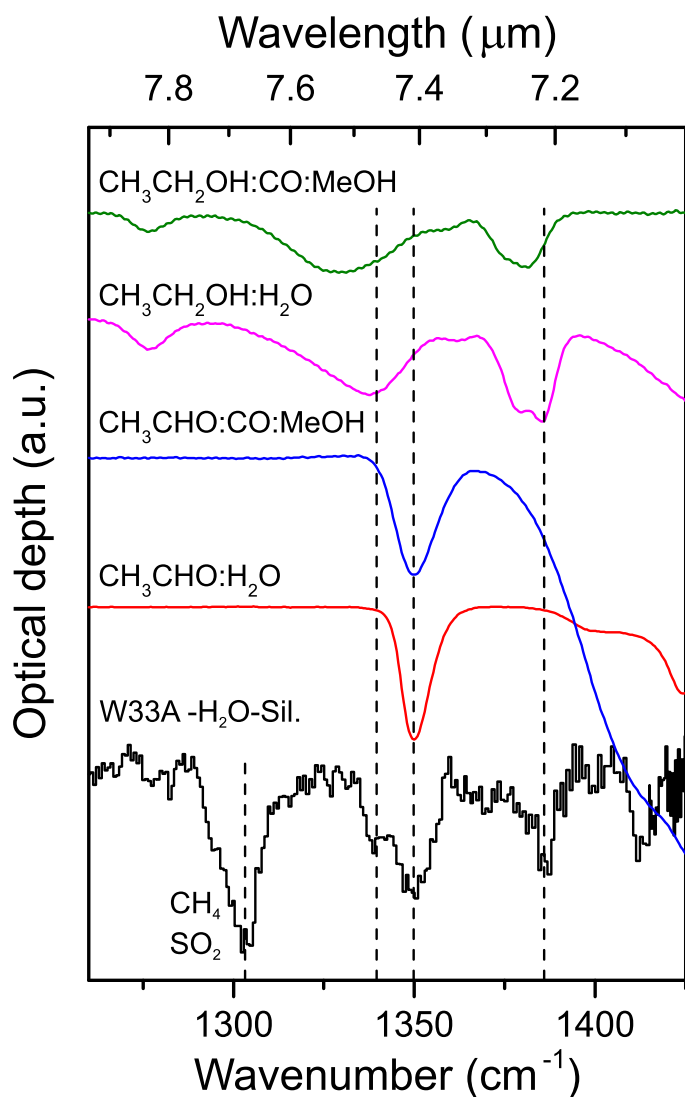
Fig. 5. Continuum and water and silicate subtracted spectrum of W33A plotted together with ice spectra of ethanol and acetaldehyde at 15 K, mixed in $CO:CH_3OH$ and H_2O. Features in the W33A spectrum are indicated with dashed lines at 7.22, 7.40, and 7.47 μm. The large spectral feature at 7.67 μm is due to CH_4 and SO_2.

Table 3. Ice upper limits and gas-phase abundances of ethanol and acetaldehyde towards W33A.

Species	Ice		Gas phase^c
	$/N(H_2O)^a$	$/N(CH_3OH)^b$	$/N(CH_3OH)$
CH_3CH_2OH	≤1.9	≤42	2.4
CH_3CHO	≤2.3	≤52	≤0.2

Notes. Abundances given in %.
References. $^{(a)}$ Keane et al. (2001). $^{(b)}$ Dartois et al. (1999). $^{(c)}$ Bisschop et al. (2007b).

strength of the CH_3 s-deformation mode in mixed ices is thus 1.8×10^{-18} cm mol^{-1}. If the entire 7.40 μm feature is attributed to CH_3CHO, the resulting column density is $8.9 \pm 3 \times 10^{17}$ cm^{-2}.

In all likelihood the 7.22 and 7.40 μm features contain contributions of other molecules, mainly HCOOH and HCOO$^-$ and the reported values should therefore be seen as upper limits. Using solid water and methanol column densities of 3.8×10^{19} and 1.7×10^{18} cm^{-2}, respectively, towards W33A (Dartois et al. 1999; Keane et al. 2001), the upper limit abundance ratios of ethanol and acetaldehyde can be determined. The abundance ratio $N(COM)/N(H_2O)$ is found to be ≤1.9% and ≤2.3%, while $N(COM)/N(CH_3OH)$ is ≤42% and ≤52% for ethanol and acetaldehyde, respectively. The abundances with respect to water are in good agreement with previously reported values of ≤4% and ≤3.6% for ethanol and acetaldehyde, respectively (Boudin et al. 1998; Schutte et al. 1999).

The $N(COM)/N(CH_3OH)$ upper limit ice abundance can be compared with known gas-phase abundances towards W33A. These are given as $N(CH_3CH_2OH)/N(CH_3OH) = 2.4\%$ and $N(CH_3CHO)/N(CH_3OH) < 0.2\%$ (Bisschop et al. 2007b) and are substantially lower than the ice upper limits. Interferometric observations with the Atacama Large Millimeter/submillimeter Array are needed to spatially resolve these molecules and determine more accurate abundances. Beside being upper limits, this difference may be linked to the process that transfers solid state species into the gas phase, causing molecules to fragment, or to other destruction of species in the gas phase. An overview of the COM abundances in ice and in the gas phase towards W33A is given in Table 3.

The spectroscopic data presented in this paper, combined with the improvements in terms of sensitivity and resolution of JWST, will aid in confirming these detections and distinguish other potential contributors to these features. More observations, particularly towards low-mass sources, will give additional information about the carriers of these features.

5. Conclusions

This paper adds to and extends on data of three important interstellar ice candidates: acetaldehyde, ethanol, and dimethyl ether. A number of selected bands are fully characterized in FWHM and peak positions and show clear changes in various matrices. Our conclusions are summarized as follows:

1. The most promising bands to identify the COMs studied here in interstellar ice spectra are the 7.427 and 5.88 μm bands of acetaldehyde, the 7.240 and 11.36 μm bands of ethanol, and the 8.011 and 8.592 μm bands of dimethyl ether.

2. Matrix characteristic shifts in peak position and FWHM are seen for several bands. The acetaldehyde CH_3 deformation

features. The ethanol band strength of the CO stretch mode at 9.514 μm has been determined to be 1.41×10^{-17} cm mol^{-1} by (Hudson 2017). Using the integrated absorbance ratio CH_3 s-def./CO str. = 0.20 at 15 K from Table B.16, the band strength of the CH_3 stretch mode is determined to be 2.8×10^{-18} cm mol^{-1}. The effect of the matrix on the relative band strength is small for both the ethanol CO stretch and CH_3 s-deformation modes, as can be seen from Figs. 3 and C.5, and therefore assumed to be negligible. Assuming the entire 7.22 μm feature is caused by ethanol, this results in a column density of $7.1 \pm 0.2 \times 10^{17}$ cm^{-2}.

In Schutte et al. (1999), the acetaldehyde band strength is given as 1.3×10^{-17} cm mol^{-1} for the CO stretch mode based on data from Wexler (1967). The integrated absorbance ratio of CO stretching/CH_3 s-deforming + CH wagging = 4.32 in pure acetaldehyde at 15 K in laboratory experiments. As the CO stretching mode is likely saturated, the ratio may thus be higher. Using this ratio, the band strength of the CH_3 s-deformation mode is found to be 3.0×10^{-18} cm mol^{-1}. As can be seen in Fig. 2, the relative band strength of this mode decreases substantially in mixtures by about 40%. The band

and CO stretching mode can be distinguished in the H_2O, CO, CH_3OH, and $CO:CH_3OH$ matrices. Ethanol shows generally less distinctive shifts and only bands in the water matrix are unique. At low temperatures matrix specific dimethyl ether band shifts can be identified, specifically for the CH_3 rocking mode at 8.011 μm.

3. Given the higher complexity of the involved spectra, unambiguous identifications need to involve different bands that reflect bandwidths and intensity ratios as found in the laboratory studies. The dependence on matrix environment and temperature provides a tool to use these transitions as a remote diagnostic instrument.

4. Analysis of the ISO W33A spectrum in the 7 μm region shows a number of features that can be assigned to the COMs studied in this work. The 7.40 μm feature matches the position of the CH_3 s-deformation mode of acetaldehyde, and the 7.22 μm feature is plausibly caused by the CH_3 s-deformation mode of ethanol. It is likely that 7.22 μm band is specifically caused by ethanol mixed in water. Abundances of both molecules with respect to water ice are determined to be ≤2.3% and ≤3.4% for acetaldehyde and ethanol, respectively.

References

Allan, A., McKean, D. C., Perchard, J.-P., & Josien, M.-L. 1971, Spectrochim. Acta A: Mol. Spectr., 27, 1409
Altwegg, K., Balsiger, H., Berthelier, J. J., et al. 2017, MNRAS, 469, S130
Baratta, G. A., & Palumbo, M. E. 1998, J. Opt. Soc. Am. A, 15, 3076
Baratta, G. A., Palumbo, M. E., & Strazzulla, G. 2000, A&A, 357, 1045
Barnes, A. J., & Hallam, H. E. 1970, Trans. Faraday Soc., 66, 1932
Bennett, C. J., Chen, S.-H., Sun, B.-J., Chang, A. H. H., & Kaiser, R. I. 2007, ApJ, 660, 1588
Bergantini, A., Maksyutenko, P., & Kaiser, R. I. 2017, ApJ, 841, 96
Bisschop, S. E., Fuchs, G. W., van Dishoeck, E. F., & Linnartz, H. 2007a, A&A, 474, 1061
Bisschop, S. E., Jørgensen, J. K., van Dishoeck, E. F., & de Wachter, E. B. M. 2007b, A&A, 465, 913
Boamah, M. D., Sullivan, K. K., Shulenberger, K. E., et al. 2014, Faraday Discuss., 168, 249
Boogert, A. C. A., Schutte, W. A., Tielens, A. G. G. M., et al. 1996, A&A, 315, L377
Boogert, A. C. A., Pontoppidan, K. M., Knez, C., et al. 2008, ApJ, 678, 985
Boogert, A. C. A., Gerakines, P. A., & Whittet, D. C. B. 2015, ARA&A, 53, 541
Bossa, J.-B., Maté, B., Fransen, C., et al. 2015, ApJ, 814, 47
Boudin, N., Schutte, W. A., & Greenberg, J. M. 1998, A&A, 331, 749
Bouilloud, M., Fray, N., Bénilan, Y., et al. 2015, MNRAS, 451, 2145
Caselli, P., & Ceccarelli, C. 2012, A&ARv, 20, 56
Cazaux, S., Tielens, A. G. G. M., Ceccarelli, C., et al. 2003, ApJ, 593, L51
Charnley, S. B. 2004, Adv. Space Res., 33, 23
Charnley, S. B., & Rodgers, S. D. 2005, in Astrochemistry: Recent Successes and Current Challenges, eds. D. C. Lis, G. A. Blake, & E. Herbst, IAU Symp., 231, 237
Coussan, S., Bouteiller, Y., & Perchard, J.P. 1998, Spectrochim. Acta A: Mol. Spectr., 102, 5789
Cuppen, H. M., Penteado, E. M., Isokoski, K., van der Marel, N., & Linnartz, H. 2011, MNRAS, 417, 2809
Dartois, E., Schutte, W., Geballe, T. R., et al. 1999, A&A, 342, L32
Dulieu, F., Amiaud, L., Congiu, E., et al. 2010, A&A, 512, A30
Ehrenfreund, P., & Charnley, S. B. 2000, ARA&A, 38, 427
Evans, J., & Bernstein, H. 1956, Can. J. Chem., 34
Fedoseev, G., Ioppolo, S., Zhao, D., Lamberts, T., & Linnartz, H. 2015, MNRAS, 446, 439
Fuchs, G. W., Cuppen, H. M., Ioppolo, S., et al. 2009, A&A, 505, 629
Gerakines, P. A., Schutte, W. A., & Ehrenfreund, P. 1996, A&A, 312, 289
Gibb, E. L., & Whittet, D. C. B. 2002, ApJ, 566, L113
Gibb, E. L., Whittet, D. C. B., Schutte, W. A., et al. 2000, ApJ, 536, 347
Gillett, F. C., & Forrest, W. J. 1973, ApJ, 179, 483
Goesmann, F., Rosenbauer, H., Bredehöft, J. H., et al. 2015, Science, 349
Herbst, E., & van Dishoeck, E. F. 2009, ARA&A, 47, 427
Hidaka, H., Watanabe, M., Kouchi, A., & Watanabe, N. 2011, Phys. Chem. Chem. Phys., 13, 15798
Hiraoka, K., Yamashita, A., Yachi, Y., et al. 1995, ApJ, 443, 363
Hollenstein, H., & Günthard, H. H. 1971, Spectrochim. Acta A: Mol. Spectr., 27, 2027
Hudson, R. L. 2017, Spectrochim. Acta A: Mol. Spectr., 187, 82
Keane, J. V., Tielens, A. G. G. M., Boogert, A. C. A., Schutte, W. A., & Whittet, D. C. B. 2001, A&A, 376, 254
Kessler, M. F., Steinz, J. A., Anderegg, M. E., et al. 1996, A&A, 315, L27
Lamberts, T., Cuppen, H. M., Ioppolo, S., & Linnartz, H. 2013, Phys. Chem. Chem. Phys., 15, 8287
Lamberts, T., Cuppen, H. M., Fedoseev, G., et al. 2014, A&A, 570, A57
Linnartz, H., Bossa, J.-B., Bouwman, J., et al. 2011, in The Molecular Universe, IAU Symp., 280, 390
Linnartz, H., Ioppolo, S., & Fedoseev, G. 2015, Int. Rev. Phys. Chem., 34, 205
Mikawa, Y., Brasch, J., & Jakobsen, R. 1971, Spectrochim. Acta A: Mol. Spectr., 27, 529
Miyauchi, N., Hidaka, H., Chigai, T., et al. 2008, Chem. Phys. Lett., 456, 27
Müller, H. S. P., Belloche, A., Xu, L.-H., et al. 2016, A&A, 587, A92
Oba, Y., Miyauchi, N., Hidaka, H., et al. 2009, ApJ, 701, 464
Oba, Y., Watanabe, N., Hama, T., et al. 2012, ApJ, 749, 67
Öberg, K. I. 2016, Chem. Rev., 116, 9631
Öberg, K. I., van Broekhuizen, F., Fraser, H. J., et al. 2005, ApJ, 621, L33
Öberg, K. I., Garrod, R. T., van Dishoeck, E. F., & Linnartz, H. 2009, A&A, 504, 891
Öberg, K. I., Boogert, A. C. A., Pontoppidan, K. M., et al. 2011, ApJ, 740, 109
Palumbo, M. E., Tielens, A. G. G. M., & Tokunaga, A. T. 1995, ApJ, 449, 674
Palumbo, M. E., Baratta, G. A., Collings, M. P., & McCoustra, M. R. S. 2006, Phys. Chem. Chem. Phys., 8, 279
Penteado, E. M., Boogert, A. C. A., Pontoppidan, K. M., et al. 2015, MNRAS, 454, 531
Plyler, E. 1952, J. Res. Natl. Bur. Stand. 48, 281
Pontoppidan, K. M. 2006, A&A, 453, L47
Posselt, W., Holota, W., Kulinyak, E., et al. 2004, in Optical, Infrared, and Millimeter Space Telescopes, ed. J. C. Mather, Proc. SPIE, 5487, 688
Schutte, W. A., Tielens, A. G. G. M., Whittet, D. C. B., et al. 1996, A&A, 315, L333
Schutte, W. A., Boogert, A. C. A., Tielens, A. G. G. M., et al. 1999, A&A, 343, 966
Taquet, V., López-Sepulcre, A., Ceccarelli, C., et al. 2015, ApJ, 804, 81
Tielens, A. G. G. M. 2013, Rev. Mod. Phys., 85, 1021
Tielens, A. G. G. M., Tokunaga, A. T., Geballe, T. R., & Baas, F. 1991, ApJ, 381, 181
Turner B. E. 1991, ApJS, 76, 617
van Broekhuizen, F. A., Keane, J. V., & Schutte, W. A. 2004, A&A, 415, 425
Watanabe, N., & Kouchi, A. 2002, ApJ, 571, L173
Werner, M. W., Roellig, T. L., Low, F. J., et al. 2004, ApJS, 154, 1
Wexler, A. 1967, Appl. Spectr. Rev., 1, 29
Wright, G. S., Wright, D., Goodson, G. B., et al. 2015, PASP, 127, 595

Appendix A: Spectra

The following figures show the spectra of acetaldehyde, ethanol, and dimethylether mixed in water, CO, methanol, and CO:methanol in the range of 2.5–20.0 μm. All spectra are taken at 15 K.
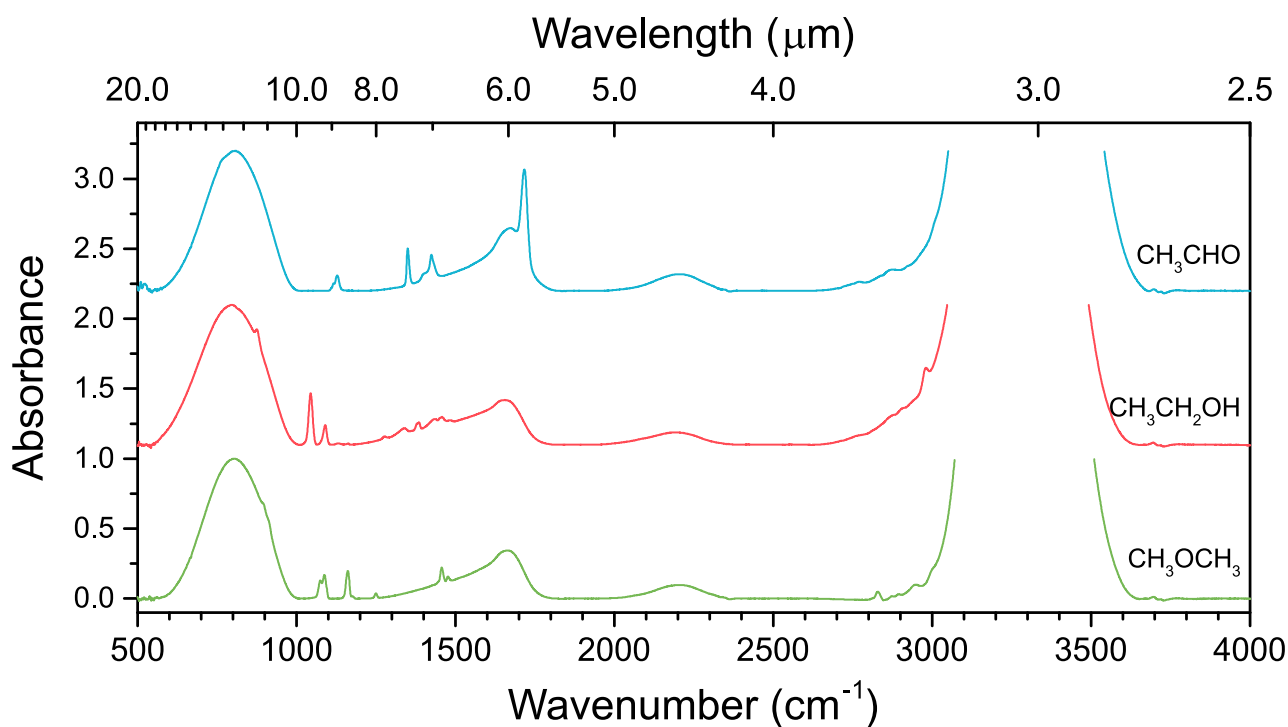
Fig. A.1. Spectra of acetaldehyde (blue), ethanol (red), and dimethyl ether (green) mixed in water at 15 K in the range of 2.5–20.0 μm.
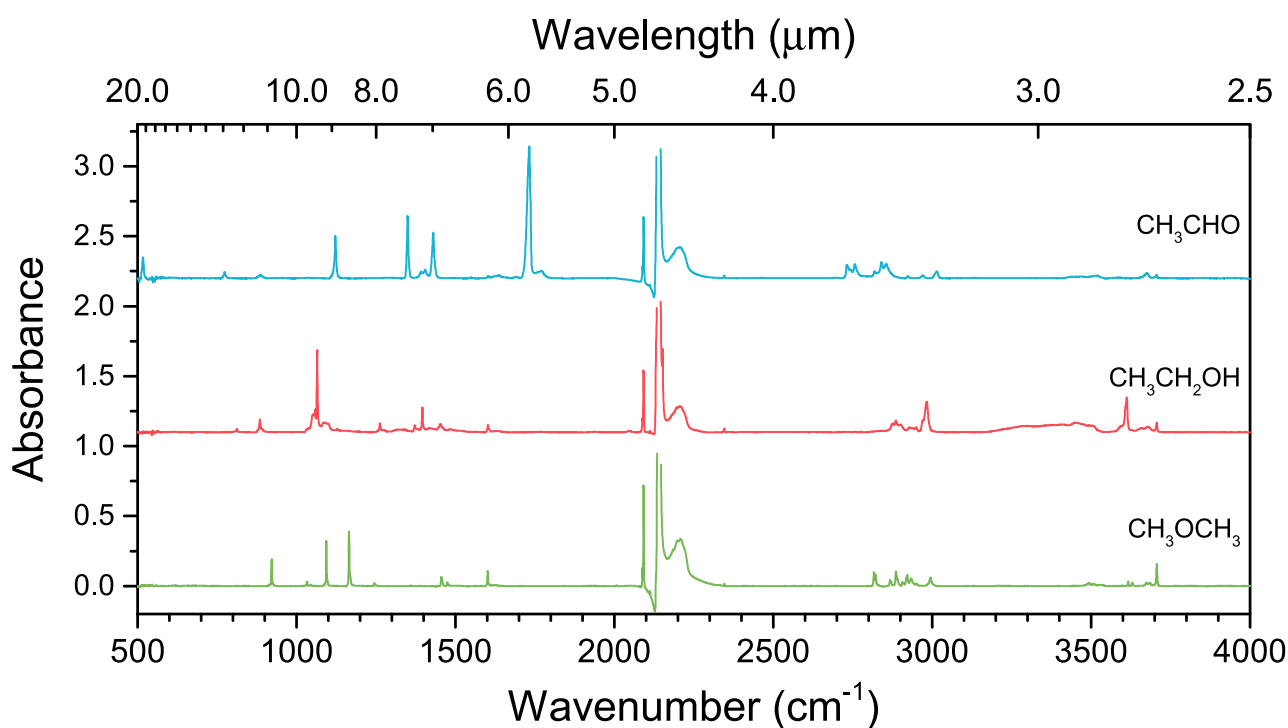
Fig. A.2. Spectra of acetaldehyde (blue), ethanol (red), and dimethyl ether (green) mixed in CO at 15 K in the range of 2.5–20.0 μm.
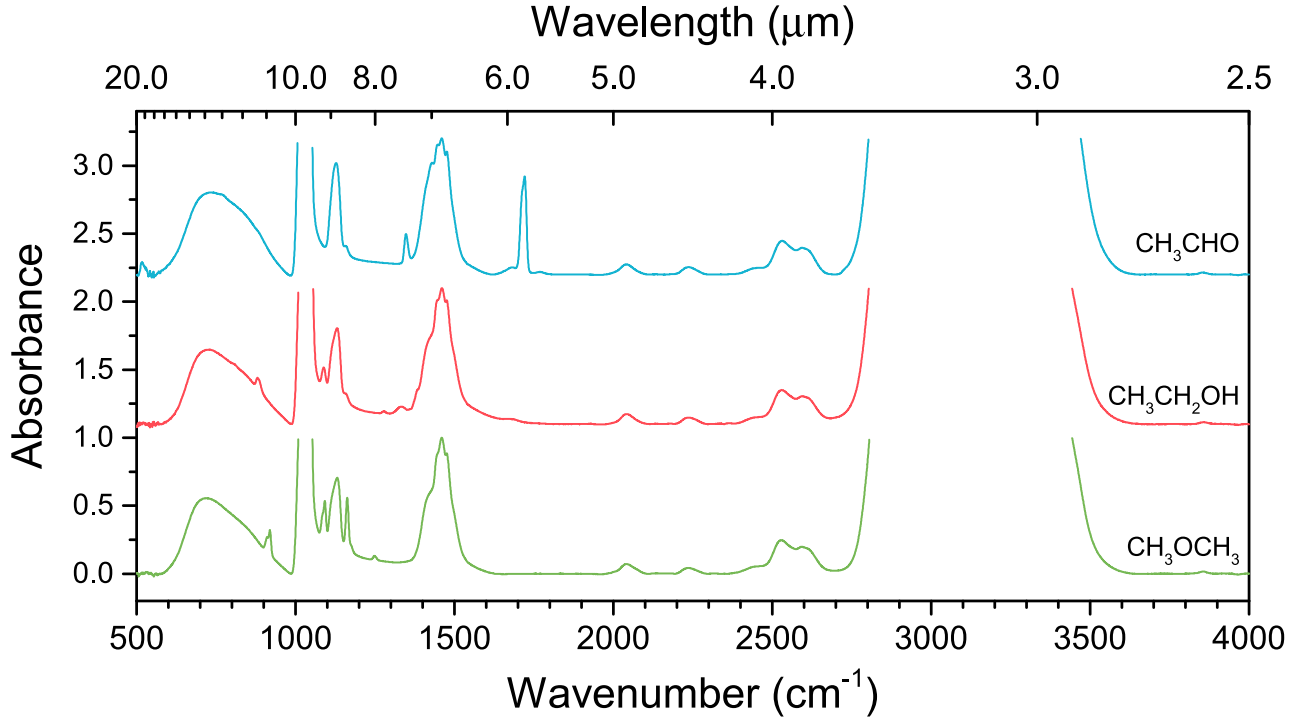
Fig. A.3. Spectra of acetaldehyde (blue), ethanol (red), and dimethyl ether (green) mixed in methanol at 15 K in the range of 2.5–20.0 μm.
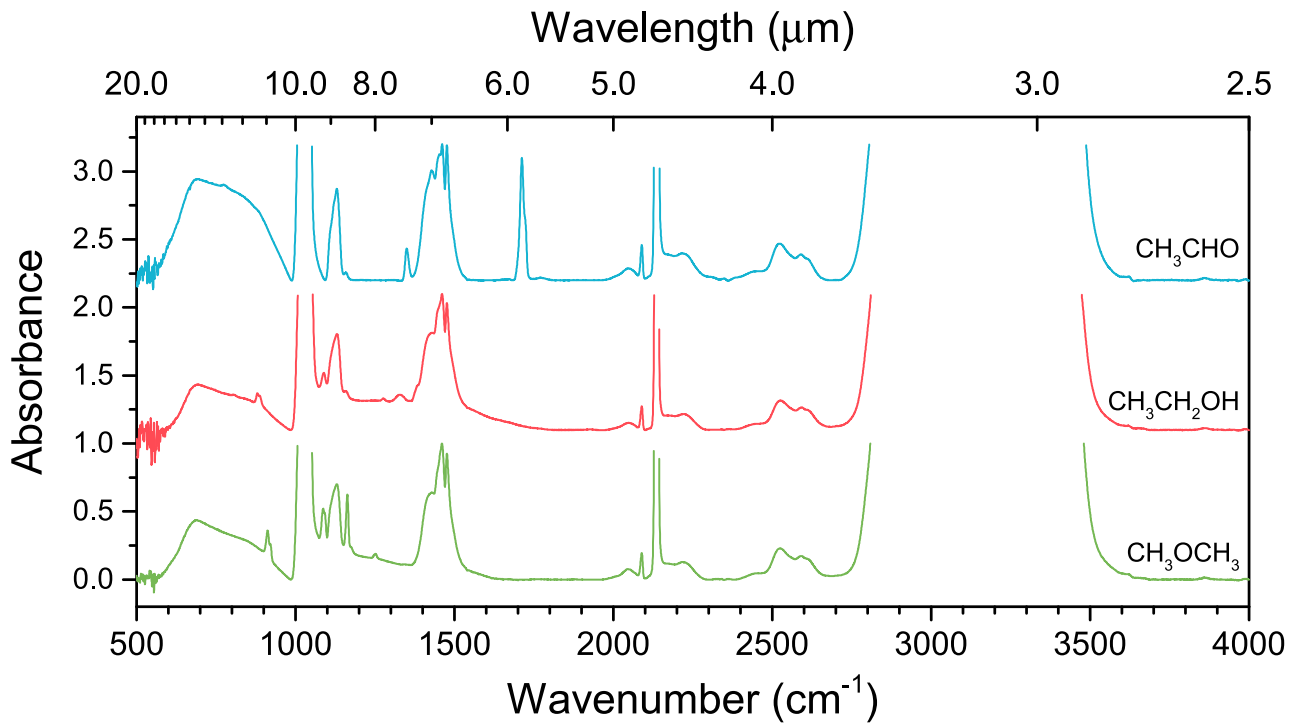
Fig. A.4. Spectra of acetaldehyde (blue), ethanol (red), and dimethyl ether (green) mixed in CO:CH_3OH at 15 K in the range of 2.5–20.0 μm.

Appendix B: Overview of peak position, FWHM, and integrated absorbance ratios of selected transitions

In this section tables are presented that list peak positions, FWHMs, and integrated absorbance ratios of selected acetaldehyde, ethanol, and dimethyl ether transitions. Where necessary, peak positions are given of both baseline corrected and matrix subtracted spectra. The peak position and FWHM are given in wavenumber (cm^{-1}) and wavelength (μm). Separate tables list the variation in band intensities over a range of temperatures for each mixture (e.g. Table B.5). Values in these tables are usually normalized to the strongest transition at 15 K, which also remains identifiable over the entire temperature range. Exceptions are made for bands that are potentially in saturation, for example the CO stretching mode in pure acetaldehyde ice.

In the tables various asterisks are used to indicate special circumstances. An asterisk indicates that the FWHM is the result of two or more blended peaks. Double asterisks indicate multiple peaks, which are often caused by a different matrix or surrounding interactions of the band. Occasionally the matrix cannot be properly subtracted from the feature under investigation, which results in FWHMs with higher uncertainty or in FWHMs that cannot be determined at all. Finally, a triple asterisks indicates ice transitions that are thought to be strong enough to saturate the IR spectrometer signal.

B.1. Acetaldehyde

Table B.1. Peak positions and FWHM of the acetaldehyde CH_3 rocking + CC stretching + CCO bending mode at $8.909\,\mu m$.

Mixture	Temperature (K)	$\lambda_{peak,-baseline}$ (cm^{-1})	(μm)	$\lambda_{peak,-matrix}$ (cm^{-1})	(μm)	FWHM (cm^{-1})	(μm)
Pure		1122.4	8.9097	–	–	13.0	0.1032
CH_3CHO:H_2O		1116.1	8.9598	1116.1	8.9598	–	–
	15	1127.7	8.8678	1127.7	8.8678	14.3	0.1121
CH_3CHO:CO		1121.9	8.9136	–	–	5.0	0.0394
CH_3CHO:CH_3OH		–	–	–	–	–	–
CH_3CHO:CO:CH_3OH		–	–	–	–	–	–
CH_3CHO		1122.4	8.9097	–	–	13.0	0.1031
CH_3CHO:H_2O		1117.5	8.9482	1117.5	8.9482	–	–
	30	1126.7	8.8754	1126.7	8.8754	14.3	0.1124
CH_3CHO:CO		1121.9	8.9136	–	–	5.5	0.0439
CH_3CHO:CH_3OH		–	–	–	–	–	–
CH_3CHO:CO:CH_3OH		–	–	–	–	–	–
CH_3CHO		1122.4	8.9097	–	–	12.5	0.0993
CH_3CHO:H_2O		1118.0	8.9443	1118.0	8.9443	–	–
	70	1124.8	8.8906	1124.8	8.8906	16.3	0.1290
CH_3CHO:CO		–	–	–	–	–	–
CH_3CHO:CH_3OH		–	–	–	–	–	–
CH_3CHO:CO:CH_3OH		–	–	–	–	–	–
CH_3CHO		1119.0	8.9366	–	–	6.4	0.0513*
		1120.9	8.9212	–	–	–	–
CH_3CHO:H_2O		1118.0	8.9443	1118.0	8.9443	–	–
	90	1124.3	8.8945	1124.3	8.8945	16.0	0.1268*
CH_3CHO:CO		–	–	–	–	–	–
CH_3CHO:CH_3OH		–	–	–	–	–	–
CH_3CHO:CO:CH_3OH		–	–	–	–	–	–
CH_3CHO		1118.5	8.9405	–	–	6.1	0.0485*
		1120.9	8.9212	–	–	–	–
CH_3CHO:H_2O		1118.0	8.9443	1118.0	8.9443	–	–
	110	1124.3	8.8945	1124.3	8.8945	16.0	0.1274*
CH_3CHO:CO		–	–	–	–	–	–
CH_3CHO:CH_3OH		–	–	–	–	–	–
CH_3CHO:CO:CH_3OH		–	–	–	–	–	–
CH_3CHO		1118.5	8.9405	–	–	5.9	0.0473
		1120.9	8.9212	–	–	–	–
CH_3CHO:H_2O		1117.5	8.9482	1117.5	8.9482	16.2	0.1291
	120	1122.4	8.9097	1122.4	8.9097	–	–
CH_3CHO:CO		–	–	–	–	–	–
CH_3CHO:CH_3OH		–	–	–	–	–	–
CH_3CHO:CO:CH_3OH		–	–	–	–	–	–
CH_3CHO		–	–	–	–	–	–
CH_3CHO:H_2O		1116.1	8.9598	1116.1	8.9598	10.0	0.0804
CH_3CHO:CO	140	–	–	–	–	–	–
CH_3CHO:CH_3OH		–	–	–	–	–	–
CH_3CHO:CO:CH_3OH		–	–	–	–	–	–
CH_3CHO		–	–	–	–	–	–
CH_3CHO:H_2O		1116.6	8.9559	1116.6	8.9559	10.1	0.0813
CH_3CHO:CO	160	–	–	–	–	–	–
CH_3CHO:CH_3OH		–	–	–	–	–	–
CH_3CHO:CO:CH_3OH		–	–	–	–	–	–

Notes. $^{(*)}$ FWHM result of two or more blended peaks. $^{(**)}$ FWHM uncertain/not determined owing to uncertain matrix subtraction. $^{(***)}$ Transition likely saturated.

Table B.2. Peak position and FWHM of the acetaldehyde CH_3 s-deformation + CH waging mode at 7.427 μm.

Mixture	Temperature (K)	$\lambda_{peak,-baseline}$		$\lambda_{peak,-matrix}$		FWHM	
		(cm^{-1})	(μm)	(cm^{-1})	(μm)	(cm^{-1})	(μm)
CH_3CHO		1346.6	7.4264	–	–	13.5	0.0744*
$CH_3CHO:H_2O$		1349.9	7.4078	1349.9	7.4078	9.2	0.0502
$CH_3CHO:CO$	15	1349.4	7.4104	–	–	4.8	0.0262
$CH_3CHO:CH_3OH$		1347.5	7.4211	–	–	13.0	0.0714
$CH_3CHO:CO:CH_3OH$		1349.4	7.4105	–	–	12.6	0.0691
CH_3CHO		1346.1	7.4290	–	–	13.7	0.0754
$CH_3CHO:H_2O$		1349.9	7.4078	1349.9	7.4078	8.8	0.0481
$CH_3CHO:CO$	30	1349.9	7.4078	–	–	6.1	0.0337*
$CH_3CHO:CH_3OH$		1347.5	7.4211	–	–	12.5	0.0686
$CH_3CHO:CO:CH_3OH$		1349.0	7.4131	–	–	12.2	0.0671
CH_3CHO		1346.1	7.4290	–	–	13.2	0.0729
$CH_3CHO:H_2O$		1349.4	7.4105	1349.4	7.4105	7.7	0.0420
$CH_3CHO:CO$	70	–	–	–	–	–	–
$CH_3CHO:CH_3OH$		1348.0	7.4184	–	–	10.9	0.0600
$CH_3CHO:CO:CH_3OH$		1348.5	7.4158	–	–	10.8	0.0592
CH_3CHO		1348.0	7.4184	–	–	7.3	0.0400*
		1351.9	7.3972	–	–	–	–
$CH_3CHO:H_2O$		1349.4	7.4105	1349.4	7.4105	7.4	0.0405
$CH_3CHO:CO$	90	–	–	–	–	–	–
$CH_3CHO:CH_3OH$		1348.0	7.4184	–	–	10.2	0.0563
$CH_3CHO:CO:CH_3OH$		1348.5	7.4158	–	–	10.6	0.0584
CH_3CHO		1348.0	7.4184	–	–	5.4	0.0298
		1351.9	7.3972	–	–	–	–
$CH_3CHO:H_2O$		1349.4	7.4105	1349.4	7.4105	7.2	0.0393
$CH_3CHO:CO$	110	–	–	–	–	–	–
$CH_3CHO:CH_3OH$		1348.0	7.4184	–	–	9.5	0.0524
$CH_3CHO:CO:CH_3OH$		1347.0	7.4237	–	–	–	–**
		1352.8	7.3920	–	–	–	–**
CH_3CHO		1348.0	7.4184	–	–	5.3	0.0291
		1352.3	7.3946	–	–	–	–
$CH_3CHO:H_2O$		1349.4	7.4105	1349.4	7.4105	7.0	0.0383
$CH_3CHO:CO$	120	–	–	–	–	–	–
$CH_3CHO:CH_3OH$		1348.0	7.4184	–	–	–	–**
$CH_3CHO:CO:CH_3OH$		1347.0	7.4237	–	–	–	–**
		1352.8	7.3920	–	–	–	–**
CH_3CHO		–	–	–	–	–	–
$CH_3CHO:H_2O$		1349.0	7.4131	1349.0	7.4131	5.7	0.0315
$CH_3CHO:CO$	140	–	–	–	–	–	–
$CH_3CHO:CH_3OH$		1347.5	7.4211	–	–	–	–**
$CH_3CHO:CO:CH_3OH$		–	–	–	–	–	–
CH_3CHO		–	–	–	–	–	–
$CH_3CHO:H_2O$		1349.0	7.4131	1349.0	7.4131	5.5	0.0302
$CH_3CHO:CO$	160	–	–	–	–	–	–
$CH_3CHO:CH_3OH$		–	–	–	–	–	–
$CH_3CHO:CO:CH_3OH$		–	–	–	–	–	–

Notes. [*] FWHM result of two or more blended peaks. [**] FWHM uncertain/not determined owing to uncertain matrix subtraction. [***] Transition likely saturated.

Table B.3. Peak position and FWHM of the acetaldehyde CH_3 deformation mode at 6.995 μm.

Mixture	Temperature (K)	$\lambda_{\text{peak},-\text{baseline}}$ (cm^{-1})	(μm)	$\lambda_{\text{peak},-\text{matrix}}$ (cm^{-1})	(μm)	FWHM (cm^{-1})	(μm)
CH_3CHO		1429.5	6.9956	–	–	22.6	0.1105
$CH_3CHO:H_2O$		1424.2	7.0216	1424.2	7.0216	17.0	0.0837
$CH_3CHO:CO$	15	1430.4	6.9909	–	–	7.7	0.0379
$CH_3CHO:CH_3OH$		–	–	–	–	–	–
$CH_3CHO:CO:CH_3OH$		–	–	–	–	–	–
CH_3CHO		1429.5	6.9956	–	–	22.8	0.1115
$CH_3CHO:H_2O$		1424.7	7.0192	1424.2	7.0216	15.7	0.0772
$CH_3CHO:CO$	30	1430.4	6.9909	–	–	9.0	0.0438
$CH_3CHO:CH_3OH$		–	–	–	–	–	–
$CH_3CHO:CO:CH_3OH$		–	–	–	–	–	–
CH_3CHO		1428.5	7.0003	–	–	22.6	0.1106
$CH_3CHO:H_2O$		1424.7	7.0192	1424.7	7.0192	14.2	0.0697
$CH_3CHO:CO$	70	–	–	–	–	–	–
$CH_3CHO:CH_3OH$		–	–	–	–	–	–
$CH_3CHO:CO:CH_3OH$		–	–	–	–	–	–
CH_3CHO		1422.7	7.0288	–	–	–	–
		1430.4	6.9909	–	–	13.3	0.0655*
$CH_3CHO:H_2O$		1425.1	7.0169	1425.1	7.0169	13.7	0.0676
$CH_3CHO:CO$	90	–	–	–	–	–	–
$CH_3CHO:CH_3OH$		–	–	–	–	–	–
$CH_3CHO:CO:CH_3OH$		–	–	–	–	–	–
CH_3CHO		1422.7	7.0288	–	–	–	–
		1430.4	6.9909	–	–	13.3	0.0653*
$CH_3CHO:H_2O$		1425.1	7.0169	1425.1	7.0169	13.1	0.0645
$CH_3CHO:CO$	110	–	–	–	–	–	–
$CH_3CHO:CH_3OH$		–	–	–	–	–	–
$CH_3CHO:CO:CH_3OH$		–	–	–	–	–	–
CH_3CHO		1422.7	7.0288	–	–	–	–
		1430.4	6.9909	–	–	13.4	0.0656*
$CH_3CHO:H_2O$		1425.1	7.0169	1425.1	7.0169	12.3	0.0603
$CH_3CHO:CO$	120	–	–	–	–	–	–
$CH_3CHO:CH_3OH$		–	–	–	–	–	–
$CH_3CHO:CO:CH_3OH$		–	–	–	–	–	–
CH_3CHO		–	–	–	–	–	–
$CH_3CHO:H_2O$		1425.1	7.0169	1425.1	7.0169	9.9	0.0488
$CH_3CHO:CO$	140	–	–	–	–	–	–
$CH_3CHO:CH_3OH$		–	–	–	–	–	–
$CH_3CHO:CO:CH_3OH$		–	–	–	–	–	–
CH_3CHO		–	–	–	–	–	–
$CH_3CHO:H_2O$		1425.1	7.0169	1424.7	7.0192	9.9	0.0488
$CH_3CHO:CO$	160	–	–	–	–	–	–
$CH_3CHO:CH_3OH$		–	–	–	–	–	–
$CH_3CHO:CO:CH_3OH$		–	–	–	–	–	–

Notes. [*] FWHM result of two or more blended peaks. [**] FWHM uncertain/not determined owing to uncertain matrix subtraction. [***] Transition likely saturated.

Table B.4. Peak position and FWHM of the acetaldehyde CO stretching mode at 5.803 μm.

Mixture	Temperature (K)	$\lambda_{peak,-baseline}$ (cm^{-1})	(μm)	$\lambda_{peak,-matrix}$ (cm^{-1})	(μm)	FWHM (cm^{-1})	(μm)
CH$_3$CHO***		1723.6	5.8019	–	–	19.5	0.0659
CH$_3$CHO:H$_2$O		1716.8	5.8247	1717.8	5.8215	20.9	0.0709
CH$_3$CHO:CO	15	1732.2	5.7729	–	–	12.6	0.0419
CH$_3$CHO:CH$_3$OH		1721.2	5.8101	–	–	20.4	0.0690
CH$_3$CHO:CO:CH$_3$OH		1712.5	5.8395	–	–	17.3	0.0589*
CH$_3$CHO***		1723.6	5.8019	–	–	20.2	0.0682
CH$_3$CHO:H$_2$O		1716.8	5.8247	1717.8	5.8215	21.2	0.0719
CH$_3$CHO:CO	30	1732.2	5.7729	–	–	12.9	–
CH$_3$CHO:CH$_3$OH		1721.6	5.8084	–	–	18.6	0.0630
CH$_3$CHO:CO:CH$_3$OH		1712.0	5.8411	–	–	19.3	0.0654*
		1722.6	5.8052	–	–	–	–
CH$_3$CHO***		1721.2	5.8101	–	–	21.1	0.0713
CH$_3$CHO:H$_2$O		1719.2	5.8166	1719.2	5.8166	20.2	0.0685
CH$_3$CHO:CO	70	–	–	–	–	–	–
CH$_3$CHO:CH$_3$OH		1722.1	5.8068	–	–	11.9	0.0401
CH$_3$CHO:CO:CH$_3$OH		1723.1	5.8035	–	–	9.2	0.0311
CH$_3$CHO***		1717.8	5.8215	–	–	18.9	0.0640*
		1722.6	5.8052	–	–	–	–
CH$_3$CHO:H$_2$O	90	1719.2	5.8166	1719.7	5.8149	19.8	0.0669
CH$_3$CHO:CO		–	–	–	–	–	–
CH$_3$CHO:CH$_3$OH		1722.6	5.8052	–	–	10.6	0.0356
CH$_3$CHO:CO:CH$_3$OH		1723.1	5.8035	–	–	9.5	0.0320
CH$_3$CHO***		1717.8	5.8215	–	–	18.2	0.0615*
		1722.6	5.8052	–	–	–	–
CH$_3$CHO:H$_2$O		1719.7	5.8149	1719.7	5.8149	20.3	0.0684
CH$_3$CHO:CO	110	–	–	–	–	–	–
CH$_3$CHO:CH$_3$OH		1723.1	5.8035	–	–	10.3	0.0347
CH$_3$CHO:CO:CH$_3$OH		1717.8	5.8215	–	–	–	–
		1720.2	5.8133	–	–	–	–
		1725.0	5.7971	–	–	13.2	0.0445*
CH$_3$CHO***		1718.3	5.8198	–	–	17.6	0.0595*
		1722.6	5.8052	–	–	–	–
CH$_3$CHO:H$_2$O		1719.7	5.8149	1720.7	5.8117	21.4	0.0722*
CH$_3$CHO:CO		–	–	–	–	–	–
CH$_3$CHO:CH$_3$OH	120	1716.8	5.8247	–	–	18.5	0.0627*
		1722.1	5.8068	–	–	–	–
CH$_3$CHO:CO:CH$_3$OH		1717.8	5.8215	–	–	–	–
		1720.2	5.8133	–	–	–	–
		1725.0	5.7971	–	–	12.3	0.0415*
CH$_3$CHO***		–	–	–	–	–	–
CH$_3$CHO:H$_2$O		1730.8	5.7777	1730.8	5.7777	17.2	0.0576*
CH$_3$CHO:CO	140	–	–	–	–	–	–
CH$_3$CHO:CH$_3$OH		1717.8	5.8215	–	9.1495	–	–
		1724.5	5.7987	–	8.5959	12.2	0.0412*
CH$_3$CHO:CO:CH$_3$OH		–	–	–	–	–	–
CH$_3$CHO***		–	–	–	–	–	–
CH$_3$CHO:H$_2$O		1731.8	5.7745	1731.8	5.7745	12.5	0.0417
CH$_3$CHO:CO	160	–	–	–	–	–	–
CH$_3$CHO:CH$_3$OH		–	–	–	–	–	–
CH$_3$CHO:CO:CH$_3$OH		–	–	–	–	–	–

Notes. [*] FWHM result of two or more blended peaks. [**] FWHM uncertain/not determined owing to uncertain matrix subtraction. [***] Transition likely saturated.

B.2. Acetaldehyde band areas

Table B.5. Integrated absorbance ratios of selected transitions in pure acetaldehyde.

Temperature	CH$_3$ rock. + CC stretch. + CCO bend.	CH$_3$ deform. + CH wag.	CH$_3$ deform.	CO stretch.
(K)	8.909 μm	7.427 μm	6.995 μm	5.803 μm
15	0.72	1.00	1.07	4.32
30	0.73	1.00	1.07	4.36
70	0.70	0.95	0.99	4.27
90	0.59	0.85	0.87	4.16
110	0.58	0.83	0.85	4.09
120	0.57	0.81	0.82	4.01

Notes. Owing to possible saturation of the C=O stretch mode the band intensities are normalized on the CH$_3$ s-deformation band at 15 K.

Table B.6. Integrated absorbance ratios of selected transitions in acetaldehyde:H$_2$O.

Temperature	CH$_3$ rock. + CC stretch. + CCO bend.	CH$_3$ deform. + CH wag.	CH$_3$ deform.	CO stretch.
(K)	8.909 μm	7.427 μm	6.995 μm	5.803 μm
15	0.15	0.21	0.27	1.00
30	0.16	0.21	0.25	1.02
70	0.15	0.21	0.22	1.00
90	0.15	0.03	0.22	1.01
110	0.15	0.19	0.20	0.94
120	0.15	0.18	0.19	0.83
140	0.12	0.15	0.17	0.61
160	0.11	0.13	0.12	0.57

Table B.7. Integrated absorbance ratios of selected transitions in acetaldehyde:CO.

Temperature	CH$_3$ rock. + CC stretch. + CCO bend.	CH$_3$ deform. + CH wag.	CH$_3$ deform.	CO stretch.
(K)	8.909 μm	7.427 μm	6.995 μm	5.803 μm
15	0.18	0.21	0.25	1.00
30	0.18	0.22	0.24	1.00

Table B.8. Integrated absorbance ratios of selected transitions in acetaldehyde:CH$_3$OH.

Temperature	CH$_3$ rock. + CC stretch. + CCO bend.	CH$_3$ deform. + CH wag.	CH$_3$ deform.	CO stretch.
(K)	8.909 μm	7.427 μm	6.995 μm	5.803 μm
15	–	0.19	–	1.00
30	–	0.19	–	0.99
70	–	0.18	–	0.95
90	–	0.17	–	0.94
110	–	0.16	–	0.96
120	–	–	–	0.62
140	–	–	–	0.35

Table B.9. Integrated absorbance ratios of selected transitions in acetaldehyde:CO:CH$_3$OH.

Temperature (K)	CH$_3$ rock. + CC stretch. + CCO bend. 8.909 μm	CH$_3$ deform. + CH wag. 7.427 μm	CH$_3$ deform. 6.995 μm	CO stretch. 5.803 μm
15	–	0.17	–	1.00
30	–	0.17	–	0.94
70	–	0.15	–	0.76
90	–	0.14	–	0.78
110	–	–	–	0.82
120	–	–	–	0.48

B.3. Ethanol

Table B.10. Peak position and FWHM of the ethanol CC stretching mode at 11.36 μm.

Mixture	Temperature (K)	$\lambda_{\text{peak},-\text{baseline}}$ (cm^{-1})	(μm)	$\lambda_{\text{peak},-\text{matrix}}$ (cm^{-1})	(μm)	FWHM (cm^{-1})	(μm)
CH_3CH_2OH		879.9	11.3654	–	–	18.3	0.2344*
CH_3CH_2OH:H_2O		875.0	11.4280	877.0	11.4029	11.7	0.1526
CH_3CH_2OH:CO	15	884.7	11.3035	–	–	3.8	0.0482
CH_3CH_2OH:CH_3OH		880.3	11.3592	882.3	11.3344	16.4	0.2105
CH_3CH_2OH:CO:CH_3OH		880.3	11.3592	880.8	11.3530	16.4	0.2097*
		887.6	11.2666	888.1	11.2605	–	–
CH_3CH_2OH		880.3	11.3592	–	–	17.9	0.2292*
CH_3CH_2OH:H_2O		874.6	11.4343	877.0	11.4029	12.1	0.1574
CH_3CH_2OH:CO	30	884.2	11.3096	–	–	4.1	0.0528
CH_3CH_2OH:CH_3OH		880.8	11.3530	882.3	11.3344	16.2	0.2074
CH_3CH_2OH:CO:CH_3OH		880.8	11.3530	880.8	11.3530	16.2	0.2073*
		888.1	11.2605	888.1	11.2605	–	–
CH_3CH_2OH		881.8	11.3406	–	–	17.3	0.2211*
CH_3CH_2OH:H_2O		874.1	11.4406	876.5	11.4092	11.8	0.1540
CH_3CH_2OH:CO	70	–	–	–	–	–	–
CH_3CH_2OH:CH_3OH		881.3	11.3468	882.8	11.3282	15.5	0.1976
CH_3CH_2OH:CO:CH_3OH		881.3	11.3468	–	–	–	–
		887.6	11.2666	888.1	11.2605	14.3	0.1830*
CH_3CH_2OH		881.8	11.3406	–	–	16.8	0.2144*
CH_3CH_2OH:H_2O		874.1	11.4406	876.5	11.4092	11.0	0.1429
CH_3CH_2OH:CO	100	–	–	–	–	–	–
CH_3CH_2OH:CH_3OH		881.3	11.3468	883.2	11.3220	14.8	0.1894
CH_3CH_2OH:CO:CH_3OH		883.2	11.3220	887.6	11.2666	14.4	0.1838*
CH_3CH_2OH		882.3	11.3344	–	–	14.2	0.1805*
		891.0	11.2240	–	–	–	–
CH_3CH_2OH:H_2O		873.1	11.4533	876.0	11.4154	11.5	0.1493
CH_3CH_2OH:CO	120	–	–	–	–	–	–
CH_3CH_2OH:CH_3OH		880.8	11.3530	882.3	11.3344	16.5	0.2107
CH_3CH_2OH:CO:CH_3OH		880.8	11.3530	883.2	11.3220	–	–
		889.5	11.2422	889.5	11.2422	18.5	0.2355*
CH_3CH_2OH		882.8	11.3282	–	–	5.2	0.0662
		891.4	11.2179	–	–	5.4	0.0678
CH_3CH_2OH:H_2O		873.6	11.4469	876.0	11.4154	11.4	0.1485
CH_3CH_2OH:CO	130	–	–	–	–	–	–
CH_3CH_2OH:CH_3OH		878.9	11.3779	882.3	11.3344	18.2	0.2319
CH_3CH_2OH:CO:CH_3OH		880.8	11.3530	883.2	11.3220	16.4	0.2098*
CH_3CH_2OH		882.8	11.3282	–	–	5.0	0.0642
		891.4	11.2179	–	–	5.2	0.0659
CH_3CH_2OH:H_2O		872.6	11.4596	876.0	11.4154	11.7	0.1518
CH_3CH_2OH:CO	140	–	–	–	–	–	–
CH_3CH_2OH:CH_3OH		880.8	11.3530	881.8	11.3406	15.4	0.1964
CH_3CH_2OH:CO:CH_3OH		880.8	11.3530	881.3	11.3468	15.1	0.1934
CH_3CH_2OH		882.8	11.3282	–	–	5.6	0.0713
		891.0	11.2240	–	–	5.5	0.0688
CH_3CH_2OH:H_2O		873.1	11.4533	876.0	11.4154	12.2	0.1582
CH_3CH_2OH:CO	150	–	–	–	–	–	–
CH_3CH_2OH:CH_3OH		880.8	11.3530	881.3	11.3468	14.0	0.1800
CH_3CH_2OH:CO:CH_3OH		880.8	11.3530	881.3	11.3468	13.6	0.1740
CH_3CH_2OH		–	–	–	–	–	–
CH_3CH_2OH:H_2O		872.1	11.4659	876.0	11.4154	12.3	0.1605
CH_3CH_2OH:CO	160	–	–	–	–	–	–
CH_3CH_2OH:CH_3OH		–	–	–	–	–	–
CH_3CH_2OH:CO:CH_3OH		–	–	–	–	–	–

Notes. [*] FWHM result of two or more blended peaks. [**] FWHM uncertain/not determined owing to uncertain matrix subtraction. [***] Transition likely saturated.

Table B.11. Peak position and FWHM of the ethanol CO stretching mode at 9.514 μm.

Mixture	Temperature (K)	$\lambda_{\text{peak,}-\text{baseline}}$ (cm^{-1})	(μm)	$\lambda_{\text{peak,}-\text{matrix}}$ (cm^{-1})	(μm)	FWHM (cm^{-1})	(μm)
CH$_3$CH$_2$OH		1051.0	9.5146	–	–	19.0	0.1724
CH$_3$CH$_2$OH:H$_2$O		1044.3	9.5761	1044.3	9.5761	14.3	0.1315
CH$_3$CH$_2$OH:CO	15	1065.0	9.3897	–	–	2.9	0.0253
CH$_3$CH$_2$OH:CH$_3$OH		–	–	–	–	–	–
CH$_3$CH$_2$OH:CO:CH$_3$OH		–	–	–	–	–	–
CH$_3$CH$_2$OH		1051.0	9.5146	–	–	17.6	0.1598
CH$_3$CH$_2$OH:H$_2$O		1044.3	9.5761	1044.3	9.5761	14.2	0.1307
CH$_3$CH$_2$OH:CO	30	1065.0	9.3897	–	–	2.8	0.0243
CH$_3$CH$_2$OH:CH$_3$OH		–	–	–	–	–	–
CH$_3$CH$_2$OH:CO:CH$_3$OH		–	–	–	–	–	–
CH$_3$CH$_2$OH		1051.0	9.5146	–	–	16.0	0.1442
CH$_3$CH$_2$OH:H$_2$O		1043.8	9.5805	1043.8	9.5805	14.0	0.1288
CH$_3$CH$_2$OH:CO	70	–	–	–	–	–	–
CH$_3$CH$_2$OH:CH$_3$OH		–	–	–	–	–	–
CH$_3$CH$_2$OH:CO:CH$_3$OH		–	–	–	–	–	–
CH$_3$CH$_2$OH		1051.0	9.5146	–	–	15.0	0.1358
CH$_3$CH$_2$OH:H$_2$O		1043.8	9.5805	1043.8	9.5805	14.0	0.1282
CH$_3$CH$_2$OH:CO	100	–	–	–	–	–	–
CH$_3$CH$_2$OH:CH$_3$OH		–	–	–	–	–	–
CH$_3$CH$_2$OH:CO:CH$_3$OH		–	–	–	–	–	–
CH$_3$CH$_2$OH		1046.2	9.5585	–	–	14.3	0.1296*
		1055.4	9.4755	–	–	–	–
CH$_3$CH$_2$OH:H$_2$O	120	1043.8	9.5805	1043.8	9.5805	14.1	0.1294
CH$_3$CH$_2$OH:CO		–	–	–	–	–	–
CH$_3$CH$_2$OH:CH$_3$OH		–	–	–	–	–	–
CH$_3$CH$_2$OH:CO:CH$_3$OH		–	–	–	–	–	–
CH$_3$CH$_2$OH		1045.7	9.5629	–	–	6.8	0.0624
		1056.3	9.4669		–	–	–
CH$_3$CH$_2$OH:H$_2$O	130	1043.8	9.5805	1043.8	9.5805	14.4	0.1325
CH$_3$CH$_2$OH:CO		–	–	–	–	–	–
CH$_3$CH$_2$OH:CH$_3$OH		–	–	–	–	–	–
CH$_3$CH$_2$OH:CO:CH$_3$OH		–	–	–	–	–	–
CH$_3$CH$_2$OH		1045.7	9.5629	–	–	6.7	0.0611
		1056.3	9.4669	–	–	6.5	0.0586
CH$_3$CH$_2$OH:H$_2$O	140	1044.3	9.5761	1044.3	9.5761	16.0	0.1469
CH$_3$CH$_2$OH:CO		–	–	–	–	–	–
CH$_3$CH$_2$OH:CH$_3$OH		–	–	–	–	–	–
CH$_3$CH$_2$OH:CO:CH$_3$OH		–	–	–	–	–	–
CH$_3$CH$_2$OH		1045.7	9.5629	–	–	7.6	0.0690
		1055.8	9.4712	–	–	–	–
CH$_3$CH$_2$OH:H$_2$O	150	1044.3	9.5761	1044.3	9.5761	17.1	0.1564
CH$_3$CH$_2$OH:CO		–	–	–	–	–	–
CH$_3$CH$_2$OH:CH$_3$OH		–	–	–	–	–	–
CH$_3$CH$_2$OH:CO:CH$_3$OH		–	–	–	–	–	–
CH$_3$CH$_2$OH		–	–	–	–	–	–
CH$_3$CH$_2$OH:H$_2$O		1044.7	9.5717	1044.7	9.5717	17.9	0.1641
CH$_3$CH$_2$OH:CO	160	–	–	–	–	–	–
CH$_3$CH$_2$OH:CH$_3$OH		–	–	–	–	–	–
CH$_3$CH$_2$OH:CO:CH$_3$OH		–	–	–	–	–	–

Notes. $^{(*)}$ FWHM result of two or more blended peaks. $^{(**)}$ FWHM uncertain/not determined owing to uncertain matrix subtraction. $^{(***)}$ Transition likely saturated.

Table B.12. Peak position and FWHM of the ethanol CH_3 rocking mode at $9.170\,\mu m$.

Mixture	Temperature (K)	$\lambda_{peak,-baseline}$ (cm^{-1})	(μm)	$\lambda_{peak,-matrix}$ (cm^{-1})	(μm)	FWHM (cm^{-1})	(μm)
CH_3CH_2OH		1090.5	9.1697	–	–	24.4	0.2057
$CH_3CH_2OH:H_2O$		1090.1	9.1738	1090.1	9.1738	12.9	0.1085
$CH_3CH_2OH:CO$	15	1084.8	9.2186	–	–	–	–
$CH_3CH_2OH:CH_3OH$		1088.6	9.1859	1088.6	9.1859	11.8	0.0996
$CH_3CH_2OH:CO:CH_3OH$		1089.6	9.1778	1087.7	9.1941	11.8	0.1001
CH_3CH_2OH		1091.0	9.1657	–	–	23.5	0.1978
$CH_3CH_2OH:H_2O$		1090.1	9.1738	1090.1	9.1738	13.0	0.1097
$CH_3CH_2OH:CO$	30	1097.8	9.1093	–	–	25.3	0.2122
$CH_3CH_2OH:CH_3OH$		1089.1	9.1819	1089.6	9.1778	11.3	0.0954
$CH_3CH_2OH:CO:CH_3OH$		1090.1	9.1738	1089.6	9.1778	11.3	0.0955
CH_3CH_2OH		1091.5	9.1616	–	–	21.4	0.1799
$CH_3CH_2OH:H_2O$		1090.1	9.1738	1090.1	9.1738	12.7	0.1067
$CH_3CH_2OH:CO$	70	–	–	–	–	–	–
$CH_3CH_2OH:CH_3OH$		1089.6	9.1778	1090.1	9.1738	11.0	0.0926
$CH_3CH_2OH:CO:CH_3OH$		1091.5	9.1616	1091.5	9.1616	10.9	0.0915
CH_3CH_2OH		1091.5	9.1616	–	–	20.6	0.1732
$CH_3CH_2OH:H_2O$		1089.6	9.1778	1089.6	9.1778	12.6	0.1064
$CH_3CH_2OH:CO$	100	–	–	–	–	–	–
$CH_3CH_2OH:CH_3OH$		1089.6	9.1778	1090.1	9.1738	10.7	0.0901
$CH_3CH_2OH:CO:CH_3OH$		1089.6	9.1778	1089.6	9.1778	10.9	0.0921
CH_3CH_2OH		1093.0	9.1495	–	–	20.4	0.1711
$CH_3CH_2OH:H_2O$		1089.6	9.1778	1089.6	9.1778	12.8	0.1076
$CH_3CH_2OH:CO$	120	–	–	–	–	–	–
$CH_3CH_2OH:CH_3OH$		1089.1	9.1819	1089.6	9.1778	10.5	0.0881
$CH_3CH_2OH:CO:CH_3OH$		1089.6	9.1778	1089.6	9.1778	10.7	0.0903
CH_3CH_2OH		1095.9	9.1253	–	–	17.8	0.1492
$CH_3CH_2OH:H_2O$		1089.6	9.1778	1089.6	9.1778	12.8	0.1080
$CH_3CH_2OH:CO$	130	–	–	–	–	–	–
$CH_3CH_2OH:CH_3OH$		1089.1	9.1819	1089.1	9.1819	10.2	0.0857
$CH_3CH_2OH:CO:CH_3OH$		1089.6	9.1778	1089.6	9.1778	9.7	0.0815
CH_3CH_2OH		1095.9	9.1253	–	–	16.9	0.1414
$CH_3CH_2OH:H_2O$		1089.6	9.1778	1089.6	9.1778	13.4	0.1127
$CH_3CH_2OH:CO$	140	–	–	–	–	–	–
$CH_3CH_2OH:CH_3OH$		1089.6	9.1778	1090.1	9.1738	12.1	0.1019
$CH_3CH_2OH:CO:CH_3OH$		1089.6	9.1778	1089.6	9.1778	12.6	0.1063
CH_3CH_2OH		1094.9	9.1334	–	–	17.2	0.1444
$CH_3CH_2OH:H_2O$		1088.6	9.1859	1088.6	9.1860	14.6	0.1230
$CH_3CH_2OH:CO$	150	–	–	–	–	–	–
$CH_3CH_2OH:CH_3OH$		1090.1	9.1738	1090.1	9.1738	12.2	0.1024
$CH_3CH_2OH:CO:CH_3OH$		1089.6	9.1778	1089.6	9.1778	12.4	0.1043
CH_3CH_2OH		–	–	–	–	–	–
$CH_3CH_2OH:H_2O$		1088.6	9.1859	1088.6	9.1859	15.1	0.1275
$CH_3CH_2OH:CO$	160	–	–	–	–	–	–
$CH_3CH_2OH:CH_3OH$		–	–	–	–	–	–
$CH_3CH_2OH:CO:CH_3OH$		–	–	–	–	–	–

Notes. [*] FWHM result of two or more blended peaks. [**] FWHM uncertain/not determined owing to uncertain matrix subtraction. [***] Transition likely saturated.

Table B.13. Peak position and FWHM of the ethanol CH_2 torsion mode at $7.842\,\mu$m.

Mixture	Temperature (K)	$\lambda_{peak,-baseline}$ (cm^{-1})	(μm)	$\lambda_{peak,-matrix}$ (cm^{-1})	(μm)	FWHM (cm^{-1})	(μm)
CH_3CH_2OH		1275.2	7.8419	–	–	18.5	0.1133
$CH_3CH_2OH:H_2O$		1278.1	7.8242	1276.2	7.8360	11.9	0.0728
$CH_3CH_2OH:CO$	15	1262.2	7.9228	–	–	3.7	0.0231
		1273.8	7.8508	–	–	–	–
$CH_3CH_2OH:CH_3OH$		1278.6	7.8212	1278.6	7.8212	12.2	0.0746
$CH_3CH_2OH:CO:CH_3OH$		1276.2	7.8360	1276.2	7.8360	11.5	0.0707
CH_3CH_2OH		1275.7	7.8390	–	–	16.9	0.1035
$CH_3CH_2OH:H_2O$		1276.2	7.8360	1276.2	7.8360	12.8	0.0784
$CH_3CH_2OH:CO$	30	1262.7	7.9198	–	–	3.1	0.0193
		1276.2	7.8360	–	–	20.6	0.1257
$CH_3CH_2OH:CH_3OH$		1278.6	7.8212	1278.6	7.8212	11.1	0.0680
$CH_3CH_2OH:CO:CH_3OH$		1276.2	7.8360	1276.2	7.8360	10.3	0.0630
CH_3CH_2OH		1276.2	7.8360	–	–	14.4	0.0881
$CH_3CH_2OH:H_2O$		1278.1	7.8242	1276.2	7.8360	12.5	0.0766
$CH_3CH_2OH:CO$	70	–	–	–	–	–	–
$CH_3CH_2OH:CH_3OH$		1278.6	7.8212	1278.6	7.8212	12.1	0.0738
$CH_3CH_2OH:CO:CH_3OH$		1278.6	7.8212	1278.6	7.8212	10.0	0.0612
CH_3CH_2OH		1276.2	7.8360	–	–	13.9	0.0853
$CH_3CH_2OH:H_2O$		1278.1	7.8242	1278.1	7.8242	13.0	0.0796
$CH_3CH_2OH:CO$	100	–	–	–	–	–	–
$CH_3CH_2OH:CH_3OH$		1278.6	7.8212	1278.6	7.8212	11.6	0.0711**
$CH_3CH_2OH:CO:CH_3OH$		1278.6	7.8212	1278.6	7.8212	12.2	0.0744
CH_3CH_2OH		1277.6	7.8271	–	–	10.5	0.0643
$CH_3CH_2OH:H_2O$		1278.1	7.8242	1276.2	7.8360	13.4	0.0823
$CH_3CH_2OH:CO$	120	–	–	–	–	–	–
$CH_3CH_2OH:CH_3OH$		1279.1	7.8183	1278.6	7.8212	9.1	0.0556**
$CH_3CH_2OH:CO:CH_3OH$		1280.5	7.8094	1278.6	7.8212	8.2	0.0501
CH_3CH_2OH		1278.1	7.8242	–	–	7.3	0.0448
$CH_3CH_2OH:H_2O$		1277.6	7.8271	1276.6	7.8330	13.5	0.0829
$CH_3CH_2OH:CO$	130	–	–	–	–	–	–
$CH_3CH_2OH:CH_3OH$		1280.5	7.8094	1278.6	7.8212	8.9	0.0547
$CH_3CH_2OH:CO:CH_3OH$		1278.6	7.8212	1278.6	7.8212	8.1	0.0495
CH_3CH_2OH		1277.6	7.8271	–	–	7.0	0.0427
$CH_3CH_2OH:H_2O$		1277.6	7.8271	1276.2	7.8360	14.0	0.0862
$CH_3CH_2OH:CO$	140	–	–	–	–	–	–
$CH_3CH_2OH:CH_3OH$		1279.1	7.8183	1278.1	7.8242	8.5	0.0519
$CH_3CH_2OH:CO:CH_3OH$		1280.5	7.8094	1276.2	7.8360	9.8	0.0604
CH_3CH_2OH		1277.6	7.8271	–	–	7.7	0.0471
$CH_3CH_2OH:H_2O$		1277.6	7.8271	1275.2	7.8419	13.5	0.0827
$CH_3CH_2OH:CO$	150	–	–	–	–	–	–
$CH_3CH_2OH:CH_3OH$		1278.1	7.8242	1276.2	7.8360	9.6	0.0590
$CH_3CH_2OH:CO:CH_3OH$		1278.6	7.8212	1276.2	7.8360	9.9	0.0609
CH_3CH_2OH		–	–	–	–	–	–
$CH_3CH_2OH:H_2O$		1277.1	7.8301	1275.2	7.8419	13.5	0.0831
$CH_3CH_2OH:CO$	160	–	–	–	–	–	–
$CH_3CH_2OH:CH_3OH$		–	–	–	–	–	–
$CH_3CH_2OH:CO:CH_3OH$		–	–	–	–	–	–

Notes. [*] FWHM result of two or more blended peaks. [**] FWHM uncertain/not determined owing to uncertain matrix subtraction. [***] Transition likely saturated.

Table B.14. Peak position and FWHM of the ethanol OH deformation mode at 7.518 μm.

Mixture	Temperature (K)	$\lambda_{peak,-baseline}$ (cm^{-1})	(μm)	$\lambda_{peak,-matrix}$ (cm^{-1})	(μm)	FWHM (cm^{-1})	(μm)
CH$_3$CH$_2$OH		1330.2	7.5179	–	–	50.9	0.2865
CH$_3$CH$_2$OH:H$_2$O		1337.9	7.4745	1337.4	7.4772	30.1	0.1690
CH$_3$CH$_2$OH:CO	15	1339.3	7.4665	–	–	40.6	0.2306*
CH$_3$CH$_2$OH:CH$_3$OH		1332.6	7.5043	1332.6	7.5043	33.6	0.1894
CH$_3$CH$_2$OH:CO:CH$_3$OH		1328.7	7.5261	1329.2	7.5233	33.7	0.1904
CH$_3$CH$_2$OH		1330.2	7.5179	–	–	48.6	0.2726
CH$_3$CH$_2$OH:H$_2$O		1337.9	7.4745	1337.9	7.4745	32.3	0.1816
CH$_3$CH$_2$OH:CO	30	1326.8	7.5370	–	–	38.4	0.2176*
CH$_3$CH$_2$OH:CH$_3$OH		1335.5	7.4880	1333.1	7.5016	35.0	0.1967
CH$_3$CH$_2$OH:CO:CH$_3$OH		1331.1	7.5125	1331.1	7.5125	30.1	0.1698
CH$_3$CH$_2$OH		1329.7	7.5206	–	–	49.4	0.2770
CH$_3$CH$_2$OH:H$_2$O		1339.8	7.4638	1337.9	7.4745	31.3	0.1758
CH$_3$CH$_2$OH:CO	70	–	–	–	–	–	–
CH$_3$CH$_2$OH:CH$_3$OH		1335.5	7.4880	1333053.0	7.5016	43.4	0.2426
CH$_3$CH$_2$OH:CO:CH$_3$OH		1335.5	7.4880	1331.1	7.5125	38.8	0.2165
CH$_3$CH$_2$OH		1329.7	7.5206	–	–	49.4	0.2770
CH$_3$CH$_2$OH:H$_2$O		1339.8	7.4638	1337.9	7.4745	31.6	0.1771
CH$_3$CH$_2$OH:CO	100	–	–	–	–	–	–
CH$_3$CH$_2$OH:CH$_3$OH		1335.5	7.4880	1331.1	7.5125	33.3	0.1875
CH$_3$CH$_2$OH:CO:CH$_3$OH		1335.5	7.4880	1331.1	7.5125	32.1	0.1807
CH$_3$CH$_2$OH		1325.3	7.5452	–	–	20.5	0.1166*
		1357.6	7.3657	–	–	–	–
CH$_3$CH$_2$OH:H$_2$O	120	1340.3	7.4611	1337.4	7.4772	32.9	0.1844
CH$_3$CH$_2$OH:CO		–	–	–	–	–	–
CH$_3$CH$_2$OH:CH$_3$OH		–	–	–	–	–	–**
CH$_3$CH$_2$OH:CO:CH$_3$OH		–	–	–	–	–	–**
CH$_3$CH$_2$OH		1324.4	7.5507	–	–	13.6	0.0778
		1357.6	7.3657	–	–	4.9	0.0264
CH$_3$CH$_2$OH:H$_2$O	130	1341.2	7.4557	1337.4	7.4772	32.8	0.1843
CH$_3$CH$_2$OH:CO		–	–	–	–	–	–
CH$_3$CH$_2$OH:CH$_3$OH		–	–	–	–	–	–**
CH$_3$CH$_2$OH:CO:CH$_3$OH		–	–	–	–	–	–**
CH$_3$CH$_2$OH		1324.4	7.5507	–	–	13.7	0.0783
		1357.6	7.3657	–	–	5.2	0.0281
CH$_3$CH$_2$OH:H$_2$O	140	1341.2	7.4557	1337.4	7.4772	34.4	0.1933
CH$_3$CH$_2$OH:CO		–	–	–	–	–	–
CH$_3$CH$_2$OH:CH$_3$OH		–	–	–	–	–	–**
CH$_3$CH$_2$OH:CO:CH$_3$OH		–	–	–	–	–	–**
CH$_3$CH$_2$OH		1324.4	7.5507	–	–	14.3	0.0819
		1357.6	7.3657	–	–	6.7	0.0362
CH$_3$CH$_2$OH:H$_2$O	150	1341.2	7.4557	1338.4	7.4719	32.4	0.1825
CH$_3$CH$_2$OH:CO		–	–	–	–	–	–
CH$_3$CH$_2$OH:CH$_3$OH		–	–	–	–	–	–**
CH$_3$CH$_2$OH:CO:CH$_3$OH		–	–	–	–	–	–**
CH$_3$CH$_2$OH		–	–	–	–	–	–
CH$_3$CH$_2$OH:H$_2$O		1341.2	7.4557	1335.0	7.4907	34.8	0.1960
CH$_3$CH$_2$OH:CO	160	–	–	–	–	–	–
CH$_3$CH$_2$OH:CH$_3$OH		–	–	–	–	–	–
CH$_3$CH$_2$OH:CO:CH$_3$OH		–	–	–	–	–	–

Notes. $^{(*)}$ FWHM result of two or more blended peaks. $^{(**)}$ FWHM uncertain/not determined owing to uncertain matrix subtraction. $^{(***)}$ Transition likely saturated.

Table B.15. Peak position and FWHM of the ethanol CH_3 s-deformation mode at $7.240\,\mu m$.

Mixture	Temperature (K)	$\lambda_{peak,-baseline}$ (cm^{-1})	(μm)	$\lambda_{peak,-matrix}$ (cm^{-1})	(μm)	FWHM (cm^{-1})	(μm)
CH_3CH_2OH		1381.3	7.2397	–	–	20.7	0.1088*
$CH_3CH_2OH:H_2O$		1379.8	7.2473	1379.3	7.2499	–	–
		1385.6	7.2171	1385.6	7.2171	15.6	0.0817
$CH_3CH_2OH:CO$	15	1372.1	7.2881	–	–	5.7	0.0304
		1396.2	7.1622	–	–	3.4	0.0175
$CH_3CH_2OH:CH_3OH$		1383.7	7.2271	1381.3	7.2397	14.9	0.0782**
$CH_3CH_2OH:CO:CH_3OH$		1384.2	7.2246	1381.7	7.2372	15.0	0.0788**
CH_3CH_2OH		1381.3	7.2397	–	–	19.8	0.1042*
$CH_3CH_2OH:H_2O$		1379.8	7.2473	1379.3	7.2499	–	–
		1385.6	7.2171	1385.1	7.2196	16.3	0.0852*
$CH_3CH_2OH:CO$	30	1372.6	7.2855	–	–	7.5	0.0397
		1383.7	7.2271	–	–	–	–
		1396.2	7.1622	–	–	3.3	0.0171
$CH_3CH_2OH:CH_3OH$		1384.2	7.2246	1381.3	7.2397	14.9	0.0784**
$CH_3CH_2OH:CO:CH_3OH$		1383.7	7.2271	1381.7	7.2372	15.9	0.0838**
CH_3CH_2OH		1380.8	7.2423	–	–	19.1	0.1005*
$CH_3CH_2OH:H_2O$		1379.3	7.2499	1379.3	7.2499	–	–
		1385.1	7.2196	1385.1	7.2196	16.7	0.0878
$CH_3CH_2OH:CO$	70	–	–	–	–	–	–
$CH_3CH_2OH:CH_3OH$		1383.2	7.2297	1380.8	7.2423	–	–
$CH_3CH_2OH:CO:CH_3OH$		1381.7	7.2372	1381.7	7.2372	16.2	0.0853**
CH_3CH_2OH		1380.3	7.2448	–	–	15.8	0.0833*
$CH_3CH_2OH:H_2O$		1379.3	7.2499	1378.9	7.2524	–	–
		1385.1	7.2196	1384.6	7.2221	17.5	0.0919*
$CH_3CH_2OH:CO$	100	–	–	–	–	–	–
$CH_3CH_2OH:CH_3OH$		1382.2	7.2347	1380.8	7.2423	15.0	0.0790**
$CH_3CH_2OH:CO:CH_3OH$		1381.7	7.2372	1381.3	7.2397	12.1	0.0635**
CH_3CH_2OH		1372.6	7.2855	–	–	15.8	0.0833
		1382.7	7.2322	–	–	–	–
$CH_3CH_2OH:H_2O$		1378.9	7.2524	1378.4	7.2549	–	–
	120	1384.6	7.2221	1384.6	7.2221	18.4	0.0967*
$CH_3CH_2OH:CO$		–	–	–	–	–	–
$CH_3CH_2OH:CH_3OH$		1381.7	7.2372	1381.3	7.2397	14.1	0.0740**
$CH_3CH_2OH:CO:CH_3OH$		1381.7	7.2372	1381.7	7.2372	12.6	0.0664**
CH_3CH_2OH		1373.1	7.2830	–	–	4.4	0.0235
		1385.1	7.2196	–	–	–	–
$CH_3CH_2OH:H_2O$		1378.4	7.2549	1378.4	7.2549	–	–
	130	1384.6	7.2221	1384.2	7.2246	18.6	0.0977*
$CH_3CH_2OH:CO$		–	–	–	–	–	–
$CH_3CH_2OH:CH_3OH$		1381.3	7.2397	1381.3	7.2397	14.6	0.0767**
$CH_3CH_2OH:CO:CH_3OH$		1381.7	7.2372	1381.7	7.2372	13.7	0.0721**
CH_3CH_2OH		1373.1	7.2830	–	–	4.5	0.0239
		1385.1	7.2196	–	–	–	–
$CH_3CH_2OH:H_2O$		1380.3	7.2448	1378.4	7.2549	19.0	0.1000*
	140	1384.2	7.2246	1383.7	7.2271	–	–
$CH_3CH_2OH:CO$		–	–	–	–	–	–
$CH_3CH_2OH:CH_3OH$		1381.3	7.2397	1381.3	7.2397	14.6	0.0769**
$CH_3CH_2OH:CO:CH_3OH$		1381.3	7.2397	1381.7	7.2372	13.9	0.0733**
CH_3CH_2OH		1373.1	7.2830	–	–	5.2	0.0277
		1384.6	7.2221	–	–	–	–
$CH_3CH_2OH:H_2O$		1380.3	7.2448	1378.4	7.2549	18.6	0.0975*
	150	1383.7	7.2271	1383.7	7.2271	–	–
$CH_3CH_2OH:CO$		–	–	–	–	–	–
$CH_3CH_2OH:CH_3OH$		1381.7	7.2372	1381.3	7.2397	14.3	0.0752**
$CH_3CH_2OH:CO:CH_3OH$		1381.7	7.2372	1381.7	7.2372	14.0	0.0734**
CH_3CH_2OH		–	–	–	–	–	–
$CH_3CH_2OH:H_2O$		1380.3	7.2448	1380.3	7.2448	18.9	0.0994
$CH_3CH_2OH:CO$	160	–	–	–	–	–	–
$CH_3CH_2OH:CH_3OH$		–	–	–	–	–	–
$CH_3CH_2OH:CO:CH_3OH$		–	–	–	–	–	–

Notes. [*] FWHM result of two or more blended peaks. [**] FWHM uncertain/not determined owing to uncertain matrix subtraction. [***] Transition likely saturated.

B.4. Ethanol normalized band areas

Table B.16. Integrated absorbance ratios of selected transitions in pure ethanol.

Temperature (K)	CC stretch. 11.36 μm	CO stretch. 9.514 μm	CH$_3$ rock. 9.170 μm	CH$_2$ tors. 7.842 μm	OH deform. 7.518 μm	CH$_3$ s-deform. 7.240 μm
15	0.23	1.00	0.59	0.06	0.35	0.20
30	0.24	1.00	0.63	0.06	0.34	0.20
70	0.24	1.00	0.65	0.06	0.38	0.23
100	0.25	1.03	0.66	0.06	0.42	0.25
120	0.28	1.04	0.64	0.05	0.47	0.23
130	0.29	1.03	0.64	0.04	0.43	0.20
140	0.28	1.02	0.64	0.04	0.44	0.21
150	0.26	0.96	0.59	0.04	0.41	0.20

Table B.17. Integrated absorbance ratios of selected transitions in ethanol:H$_2$O.

Temperature (K)	CC stretch. 11.36 μm	CO stretch. 9.514 μm	CH$_3$ rock. 9.170 μm	CH$_2$ tors. 7.842 μm	OH deform. 7.518 μm	CH$_3$ s-deform. 7.240 μm
15	0.16	1.00	0.35	0.04	0.24	0.17
30	0.17	1.01	0.35	0.05	0.28	0.19
70	0.16	1.01	0.34	0.05	0.28	0.20
100	0.12	0.97	0.33	0.05	0.30	0.21
120	0.12	0.93	0.33	0.05	0.30	0.21
130	0.12	0.93	0.33	0.04	0.27	0.21
140	0.11	0.88	0.35	0.04	0.26	0.20
150	0.11	0.86	0.36	0.04	0.21	0.16
160	0.09	0.74	0.32	0.03	0.17	0.14

Table B.18. Integrated absorbance ratios of selected transitions in ethanol:CH$_3$OH.

Temperature (K)	CC stretch. 11.36 μm	CO stretch. 9.514 μm	CH$_3$ rock. 9.170 μm	CH$_2$ tors. 7.842 μm	OH deform. 7.518 μm	CH$_3$ s-deform. 7.240 μm
15	1.00	–	0.99	0.16	1.50	0.57
30	1.00	–	1.09	0.16	1.83	0.62
70	1.01	–	1.38	0.19	3.14	0.81
100	1.00	–	1.36	0.18	2.38	0.66
120	1.05	–	1.12	0.18	–	0.85
130	0.97	–	0.92	0.10	–	0.67
140	0.98	–	1.12	0.09	–	0.66
150	0.90	–	0.99	0.10	–	0.54

Table B.19. Integrated absorbance ratios of selected transitions in ethanol:CO:CH$_3$OH.

Temperature (K)	CC stretch. 11.36 μm	CO stretch. 9.514 μm	CH$_3$ rock. 9.170 μm	CH$_2$ tors. 7.842 μm	OH deform. 7.518 μm	CH$_3$ s-deform. 7.240 μm
15	1.00	–	0.87	0.19	1.73	0.66
30	1.00	–	1.09	0.19	1.89	0.91
70	0.94	–	1.37	0.19	2.80	0.79
100	0.94	–	1.39	0.23	2.40	0.69
120	0.77	–	1.03	0.11	–	0.61
130	0.87	–	1.20	0.11	–	0.62
140	0.90	–	1.16	0.12	–	0.57
150	0.89	–	1.06	0.12	–	0.54

B.5. Dimethyl ether

Table B.20. Peak position and FWHM of the dimethyl ether COC stretching mode at $10.85\,\mu$m.

Mixture	Temperature (K)	$\lambda_{\mathrm{peak,-baseline}}$ (cm^{-1})	(μm)	$\lambda_{\mathrm{peak,-matrix}}$ (cm^{-1})	(μm)	FWHM (cm^{-1})	(μm)
CH$_3$OCH$_3$		921.8	10.8483	–	–	10.6	0.1245
CH$_3$OCH$_3$:H$_2$O		898.2	11.1336	898.2	11.1336	–	–
		913.1	10.9514	913.1	10.9514	27.9	0.3406*
CH$_3$OCH$_3$:CO	15	921.8	10.8483	–	–	2.1	0.0248
CH$_3$OCH$_3$:CH$_3$OH		911.2	10.9745	911.7	10.9687	–	–
		919.4	10.8767	919.4	10.8767	15.5	0.1846*
CH$_3$OCH$_3$:CO:CH$_3$OH		912.2	10.9629	912.6	10.9571	15.9	0.1904*
		920.8	10.8596	921.3	10.8539	–	–
CH$_3$OCH$_3$		921.3	10.8539	–	–	10.6	0.1243
CH$_3$OCH$_3$:H$_2$O		897.7	11.1396	898.2	11.1336	–	–
		914.1	10.9398	913.6	10.9456	27.5	0.3358*
CH$_3$OCH$_3$:CO	30	921.8	10.8483	–	–	2.2	0.0253
CH$_3$OCH$_3$:CH$_3$OH		911.2	10.9745	911.7	10.9687	–	–
		919.4	10.8767	919.9	10871.0000	9.0	0.1062
CH$_3$OCH$_3$:CO:CH$_3$OH		912.6	10.9571	912.6	10.9571	16.2	0.1933*
		921.3	10.8539	921.3	10.8539	–	–
CH$_3$OCH$_3$		914.1	10.9398	–	–	–	–
		918.0	10.8938	–	–	4.1	0.0492
CH$_3$OCH$_3$:H$_2$O		896.3	11.1575	898.2	11.1336	–	–
		913.6	10.9456	913.6	10.9456	15.2	0.1834
CH$_3$OCH$_3$:CO	70	–	–	–	–	–	–
CH$_3$OCH$_3$:CH$_3$OH		910.7	10.9803	911.2	10.9745	–	–
		919.9	10.8710	919.9	10.8710	6.9	0.0815
CH$_3$OCH$_3$:CO:CH$_3$OH		911.2	10.9745	911.2	10.9745	–	–
		920.4	10.8653	920.4	10.8653	6.1	0.0723
CH$_3$OCH$_3$		914.1	10.9398	–	–	–	–
		918.0	10.8938	–	–	6.3	0.0755*
CH$_3$OCH$_3$:H$_2$O		–	–	898.7	11.1276	–	–
		913.6	10.9456	913.6	10.9456	15.0	0.1807
CH$_3$OCH$_3$:CO	90	–	–	–	–	–	–
CH$_3$OCH$_3$:CH$_3$OH		910.7	10.9803	911.2	10.9745	–	–
		919.9	10.8710	920.4	10.8653	6.4	0.0760
CH$_3$OCH$_3$:CO:CH$_3$OH		911.2	10.9745	911.2	10.9745	–	–
		919.9	10.8710	919.9	10.8710	6.4	0.0755
CH$_3$OCH$_3$		914.6	10.9340	–	–	–	–
		918.0	10.8938	–	–	6.3	0.0744
CH$_3$OCH$_3$:H$_2$O		–	–	898.2	11.1336	–	–
		913.1	10.9514	913.6	10.9456	14.0	0.1688
CH$_3$OCH$_3$:CO	100	–	–	–	–	–	–
CH$_3$OCH$_3$:CH$_3$OH		910.7	10.9803	910.7	10.9803	–	–
		920.4	10.8653	920.4	10.8653	6.3	0.0744
CH$_3$OCH$_3$:CO:CH$_3$OH		911.2	10.9745	911.2	10.9745	–	–
		920.4	10.8653	920.4	10.8653	6.4	0.0754
CH$_3$OCH$_3$		–	–	–	–	–	–
CH$_3$OCH$_3$:H$_2$O		912.6	10.9571	913.6	10.9456	13.8	0.1656
CH$_3$OCH$_3$:CO	120	–	–	–	–	–	–
CH$_3$OCH$_3$:CH$_3$OH		907.3	11.0212	911.7	10.9687	–	–
		918.4	10.8881	919.4	10.8767	19.5	0.2327
CH$_3$OCH$_3$:CO:CH$_3$OH		–	–	–	–	–	–
CH$_3$OCH$_3$		–	–	–	–	–	–
CH$_3$OCH$_3$:H$_2$O		912.6	10.9571	914.6	10.9340	13.9	0.1659
CH$_3$OCH$_3$:CO	140	–	–	–	–	–	–
CH$_3$OCH$_3$:CH$_3$OH		–	–	–	–	–	–
CH$_3$OCH$_3$:CO:CH$_3$OH		–	–	–	–	–	–
CH$_3$OCH$_3$		–	–	–	–	–	–
CH$_3$OCH$_3$:H$_2$O		913.1	10.9514	913.1	10.9514	13.2	0.1580
CH$_3$OCH$_3$:CO	160	–	–	–	–	–	–
CH$_3$OCH$_3$:CH$_3$OH		–	–	–	–	–	–
CH$_3$OCH$_3$:CO:CH$_3$OH		–	–	–	–	–	–

Notes. [*] FWHM result of two or more blended peaks. [**] FWHM uncertain/not determined owing to uncertain matrix subtraction. [***] Transition likely saturated.

Table B.21. Peak position and FWHM of the dimethyl ether COC stretching + CH_3 rocking mode at 9.141 μm.

Mixture	Temperature (K)	$\lambda_{peak,-baseline}$ (cm^{-1})	(μm)	$\lambda_{peak,-matrix}$ (cm^{-1})	(μm)	FWHM (cm^{-1})	(μm)
CH_3OCH_3		1094.4	9.1374	–	–	10.9	0.0912
CH_3OCH_3:H_2O		1074.6	9.3055	1074.6	9.3055	–	–
	15	1087.7	9.1941	1088.1	9.1900	24.7	0.2111*
CH_3OCH_3:CO		1093.9	9.1414	–	–	2.0	0.0168
CH_3OCH_3:CH_3OH		1092.0	9.1576	1092.0	9.1576	12.5	0.1055*
CH_3OCH_3:CO:CH_3OH		1087.2	9.1982	1087.2	9.1982	13.8	0.1162
CH_3OCH_3		1093.9	9.1414	–	–	10.9	0.0909
CH_3OCH_3:H_2O		1074.2	9.3096	1074.2	9.3096	–	–
		1087.7	9.1941	1087.7	9.1941	23.4	0.1994*
CH_3OCH_3:CO	30	1094.4	9.1374	–	–	2.2	0.0182
CH_3OCH_3:CH_3OH		1092.5	9.1535	1092.5	9.1535	8.6	0.0723*
CH_3OCH_3:CO:CH_3OH		1086.7	9.2023	1086.7	9.2023	–	–
		1093.0	9.1495	1093.0	9.1495	14.2	0.1195*
CH_3OCH_3***		1091.5	9.1616	–	–	3.9	0.0326
CH_3OCH_3:H_2O		1074.2	9.3096	1074.2	9.3096	–	–
		1088.1	9.1900	1088.6	9.1860	11.8	0.0997
	70						
CH_3OCH_3:CO		–	–	–	–	–	–
CH_3OCH_3:CH_3OH		1093.0	9.1495	1093.0	9.1495	6.6	0.0554
CH_3OCH_3:CO:CH_3OH		1093.0	9.1495	1093.0	9.1495	6.1	0.0508
CH_3OCH_3***		1091.5	9.1616	–	–	3.6	0.0299
CH_3OCH_3:H_2O		1074.2	9.3096	1074.2	9.3096	–	–
		1088.6	9.1859	1088.6	9.1859	11.3	0.0957
	90						
CH_3OCH_3:CO		–	–	–	–	–	–
CH_3OCH_3:CH_3OH		1093.0	9.1495	1093.0	9.1495	6.2	0.0517
CH_3OCH_3:CO:CH_3OH		1093.0	9.1495	1093.0	9.1495	6.2	0.0515
CH_3OCH_3***		1091.5	9.1616	–	–	3.5	0.0294
CH_3OCH_3:H_2O		1073.7	9.3138	1072.7	9.3222	–	–
		1088.6	9.1859	1088.6	9.1859	11.1	0.0940
	100						
CH_3OCH_3:CO		–	–	–	–	–	–
CH_3OCH_3:CH_3OH		1093.0	9.1495	1093.0	9.1495	6.0	0.0506
CH_3OCH_3:CO:CH_3OH		1093.0	9.1495	1093.0	9.1495	6.2	0.0522
CH_3OCH_3***		–	–	–	–	–	–
CH_3OCH_3:H_2O		1073.7	9.3138	1073.2	9.3180	–	–
		1088.6	9.1859	1088.6	9.1859	12.1	0.1016
CH_3OCH_3:CO	120	–	–	–	–	–	–
CH_3OCH_3:CH_3OH		1084.8	9.2186	1085.2	9.2145	–	–
		1093.0	9.1495	1093.4	9.1454	15.5	0.1305
CH_3OCH_3:CO:CH_3OH		–	–	–	–	–	–
CH_3OCH_3***		–	–	–	–	–	–
CH_3OCH_3:H_2O		1089.6	9.1778	1089.6	9.1778	–	–
		1095.9	9.1253	1095.9	9.1253	13.3	0.1121
	140						
CH_3OCH_3:CO		–	–	–	–	–	–
CH_3OCH_3:CH_3OH		–	–	–	–	–	–
CH_3OCH_3:CO:CH_3OH		–	–	–	–	–	–
CH_3OCH_3***		–	–	–	–	–	–
CH_3OCH_3:H_2O		1090.5	9.1697	1090.5	9.1697	–	–
		1095.9	9.1253	1095.9	9.1253	10.9	0.0911
	160						
CH_3OCH_3:CO		–	–	–	–	–	–
CH_3OCH_3:CH_3OH		–	–	–	–	–	–
CH_3OCH_3:CO:CH_3OH		–	–	–	–	–	–

Notes. $^{(*)}$ FWHM result of two or more blended peaks. $^{(**)}$ FWHM uncertain/not determined owing to uncertain matrix subtraction. $^{(***)}$ Transition likely saturated.

Table B.22. Peak position and FWHM of the dimethyl ether COC stretching and CH_3 rocking mode at $8.592\,\mu m$.

Mixture	Temperature (K)	$\lambda_{peak,-baseline}$ (cm^{-1})	(μm)	$\lambda_{peak,-matrix}$ (cm^{-1})	(μm)	FWHM (cm^{-1})	(μm)
CH_3OCH_3		1164.3	8.5888	–	–	9.7	0.0714
CH_3OCH_3:H_2O		1161.4	8.6102	1161.4	8.6102	12.5	0.0924
CH_3OCH_3:CO	15	1165.3	8.5817	–	–	2.4	0.0177
CH_3OCH_3:CH_3OH		1162.9	8.5994	1162.9	8.5994	9.6	0.0712
CH_3OCH_3:CO:CH_3OH		1163.3	8.5959	1163.3	8.5959	8.2	0.0608
CH_3OCH_3		1163.8	8.5923	–	–	9.7	0.0712
CH_3OCH_3:H_2O		1161.9	8.6066	1161.9	8.6066	12.1	0.0895
CH_3OCH_3:CO	30	1165.8	8.5781	–	–	2.7	0.0196
CH_3OCH_3:CH_3OH		1162.9	8.5994	1162.9	8.5994	9.0	0.0668
CH_3OCH_3:CO:CH_3OH		1163.3	8.5959	1163.3	8.5959	7.8	0.0578
CH_3OCH_3***		1163.8	8.5923	–	–	3.9	0.0291
CH_3OCH_3:H_2O		1162.4	8.6030	1162.4	8.6030	10.2	0.0759
CH_3OCH_3:CO	70	–	–	–	–	–	–
CH_3OCH_3:CH_3OH		1162.9	8.5994	1163.3	8.5959	7.8	0.0576
CH_3OCH_3:CO:CH_3OH		1163.8	8.5923	1163.8	8.5923	7.0	0.0514
CH_3OCH_3***		1163.8	8.5923	–	–	3.6	0.0268
CH_3OCH_3:H_2O		1162.4	8.6030	1162.4	8.6030	9.4	0.0697
CH_3OCH_3:CO	90	–	–	–	–	–	–
CH_3OCH_3:CH_3OH		1163.3	8.5959	1163.3	8.5959	7.2	0.0534
CH_3OCH_3:CO:CH_3OH		1163.3	8.5959	1163.3	8.5959	7.2	0.0531
CH_3OCH_3***		1163.8	8.5923	–	–	3.7	0.0270
CH_3OCH_3:H_2O		1162.4	8.6030	1162.9	8.5994	9.1	0.0673
CH_3OCH_3:CO	100	–	–	–	–	–	–
CH_3OCH_3:CH_3OH		1163.3	8.5959	1163.3	8.5959	7.1	0.0522
CH_3OCH_3:CO:CH_3OH		1163.3	8.5959	1163.3	8.5959	7.2	0.0535
CH_3OCH_3		–	–	–	–	–	–
CH_3OCH_3:H_2O		1163.3	8.5959	1163.3	8.5959	8.8	0.0651
CH_3OCH_3:CO	120	–	–	–	–	–	–
CH_3OCH_3:CH_3OH		1160.9	8.6137	1161.4	8.6102	10.4	0.0770
CH_3OCH_3:CO:CH_3OH		–	–	–	–	–	–
CH_3OCH_3		–	–	–	–	–	–
CH_3OCH_3:H_2O		1165.8	8.5781	1165.8	8.5781	9.0	0.0661
CH_3OCH_3:CO	140	–	–	–	–	–	–
CH_3OCH_3:CH_3OH		–	–	–	–	–	–
CH_3OCH_3:CO:CH_3OH		–	–	–	–	–	–
CH_3OCH_3		–	–	–	–	–	–
CH_3OCH_3:H_2O		1167.2	8.5675	1167.2	8.5675	8.8	0.0648
CH_3OCH_3:CO	160	–	–	–	–	–	–
CH_3OCH_3:CH_3OH		–	–	–	–	–	–
CH_3OCH_3:CO:CH_3OH		–	–	–	–	–	–

Notes. [*] FWHM result of two or more blended peaks. [**] FWHM uncertain/not determined owing to uncertain matrix subtraction. [***] Transition likely saturated.

Table B.23. Peak position and FWHM of the dimethyl ether CH$_3$ rocking mode at 8.011 μm.

Mixture	Temperature (K)	$\lambda_{\text{peak},-\text{baseline}}$ (cm^{-1})	(μm)	$\lambda_{\text{peak},-\text{matrix}}$ (cm^{-1})	(μm)	FWHM (cm^{-1})	(μm)
CH$_3$OCH$_3$		1248.2	8.0115	–	–	9.6	0.0617
CH$_3$OCH$_3$:H$_2$O		1250.1	7.9992	1250.1	7.9992	8.4	0.0540
CH$_3$OCH$_3$:CO	15	1244.8	8.0333	–	–	2.8	0.0180
CH$_3$OCH$_3$:CH$_3$OH		1247.7	8.0146	1247.7	8.0146	11.9	0.0761
CH$_3$OCH$_3$:CO:CH$_3$OH		1251.6	7.9899	1251.6	7.9899	11.4	0.0728
CH$_3$OCH$_3$		1248.2	8.0115	–	–	9.6	0.0614
CH$_3$OCH$_3$:H$_2$O		1249.6	8.0023	1249.6	8.0023	8.3	0.0534
CH$_3$OCH$_3$:CO	30	1245.3	8.0301	–	–	3.1	0.0200
CH$_3$OCH$_3$:CH$_3$OH		1247.7	8.0146	1247.7	8.0146	11.1	0.0710
CH$_3$OCH$_3$:CO:CH$_3$OH		1252.1	7.9869	1252.1	7.9869	12.1	0.0775
CH$_3$OCH$_3$		1250.1	7.9992	–	–	3.4	0.0219
CH$_3$OCH$_3$:H$_2$O		1249.6	8.0023	1249.6	8.0023	7.6	0.0484
CH$_3$OCH$_3$:CO	70	–	–	–	–	–	–
CH$_3$OCH$_3$:CH$_3$OH		1246.8	8.0209	1246.8	8.0208	9.7	0.0624
CH$_3$OCH$_3$:CO:CH$_3$OH		1245.8	8.0270	1245.8	8.0270	7.4	0.0478
CH$_3$OCH$_3$		1249.6	8.0023	–	–	3.4	0.0221
CH$_3$OCH$_3$:H$_2$O		1249.6	8.0023	1249.6	8.0023	7.7	0.0490
CH$_3$OCH$_3$:CO	90	–	–	–	–	–	–
CH$_3$OCH$_3$:CH$_3$OH		1245.8	8.0270	1245.8	8.0270	8.5	0.0546
CH$_3$OCH$_3$:CO:CH$_3$OH		1245.3	8.0301	1245.3	8.0301	7.8	0.0502
CH$_3$OCH$_3$		1249.2	8.0054	–	–	3.5	0.0226
CH$_3$OCH$_3$:H$_2$O		1249.6	8.0023	1249.6	8.0023	7.5	0.0479
CH$_3$OCH$_3$:CO	100	–	–	–	–	–	–
CH$_3$OCH$_3$:CH$_3$OH		1245.8	8.0270	1245.8	8.0270	8.7	0.0559
CH$_3$OCH$_3$:CO:CH$_3$OH		1245.3	8.0301	1245.3	8.0301	9.8	0.0630
CH$_3$OCH$_3$		–	–	–	–	–	–
CH$_3$OCH$_3$:H$_2$O		1249.6	8.0023	1249.6	8.0023	7.7	0.0493
CH$_3$OCH$_3$:CO	120	–	–	–	–	–	–
CH$_3$OCH$_3$:CH$_3$OH		1248.2	8.0115	1247.7	8.0146	9.6	0.0614
CH$_3$OCH$_3$:CO:CH$_3$OH		–	–	–	–	–	–
CH$_3$OCH$_3$		–	–	–	–	–	–
CH$_3$OCH$_3$:H$_2$O		1249.2	8.0054	1249.2	8.0054	8.3	0.0530
CH$_3$OCH$_3$:CO	140	–	–	–	–	–	–
CH$_3$OCH$_3$:CH$_3$OH		–	–	–	–	–	–
CH$_3$OCH$_3$:CO:CH$_3$OH		–	–	–	–	–	–
CH$_3$OCH$_3$		–	–	–	–	–	–
CH$_3$OCH$_3$:H$_2$O		1248.7	8.0084	1248.7	8.0084	8.7	0.0556
CH$_3$OCH$_3$:CO	160	–	–	–	–	–	–
CH$_3$OCH$_3$:CH$_3$OH		–	–	–	–	–	–
CH$_3$OCH$_3$:CO:CH$_3$OH		–	–	–	–	–	–

Notes. [*] FWHM result of two or more blended peaks. [**] FWHM uncertain/not determined owing to uncertain matrix subtraction. [***] Transition likely saturated.

B.6. Dimethyl ether band areas

Table B.24. Integrated absorbance ratios of selected transitions in pure dimethyl ether.

Temperature (K)	COC stretch. 10.85 μm	COC stretch. + CH$_3$ rock. 9.141 μm	COC stretch. + CH$_3$ rock. 8.592 μm	CH$_3$ rock. 8.011 μm
15	0.49	0.83	1.00	0.06
30	0.49	0.83	0.99	0.07
70	0.48	0.79	0.85	0.06
90	0.48	0.78	0.84	0.06
100	0.46	0.74	0.80	0.06

Table B.25. Integrated absorbance ratios of selected transitions in dimethyl ether:H$_2$O.

Temperature (K)	COC stretch. 10.85 μm	COC stretch. + CH$_3$ rock. 9.141 μm	COC stretch. + CH$_3$ rock. 8.592 μm	CH$_3$ rock. 8.011 μm
15	0.36	1.00	0.74	0.08
30	0.40	0.99	0.80	0.08
70	0.38	0.94	0.79	0.07
90	0.37	0.91	0.78	0.07
100	0.34	0.89	0.78	0.07
120	0.30	0.84	0.80	0.06
140	0.17	0.71	0.79	0.05
160	0.10	0.61	0.73	0.04

Table B.26. Integrated absorbance ratios of selected transitions in dimethyl ether:CO.

Temperature (K)	COC stretch. 10.85 μm	COC stretch. + CH$_3$ rock. 9.141 μm	COC stretch. + CH$_3$ rock. 8.592 μm	CH$_3$ rock. 8.011 μm
15	0.45	0.66	1.00	0.06
30	0.45	0.70	1.00	0.07

Table B.27. Integrated absorbance ratios of selected transitions in dimethyl ether:CH$_3$OH.

Temperature (K)	COC stretch. 10.85 μm	COC stretch. + CH$_3$ rock. 9.141 μm	COC stretch. + CH$_3$ rock. 8.592 μm	CH$_3$ rock. 8.011 μm
15	0.71	0.71	1.00	0.10
30	0.69	0.77	1.04	0.09
70	0.65	0.83	1.04	0.09
90	0.63	0.84	1.08	0.08
100	0.60	0.82	1.05	0.08
120	0.29	0.39	0.38	0.04

Table B.28. Integrated absorbance ratios of selected transitions in dimethyl ether:CO:CH$_3$OH.

Temperature (K)	COC stretch. 10.85 μm	COC stretch. + CH$_3$ rock. 9.141 μm	COC stretch. + CH$_3$ rock. 8.592 μm	CH$_3$ rock. 8.011 μm
15	0.81	0.88	1.00	0.13
30	0.83	1.02	1.13	0.12
70	0.63	0.86	1.04	0.08
90	0.63	0.83	1.00	0.08
100	0.51	0.67	0.77	0.07

Appendix C: Spectroscopic data of selected bands

C.1. Acetaldehyde
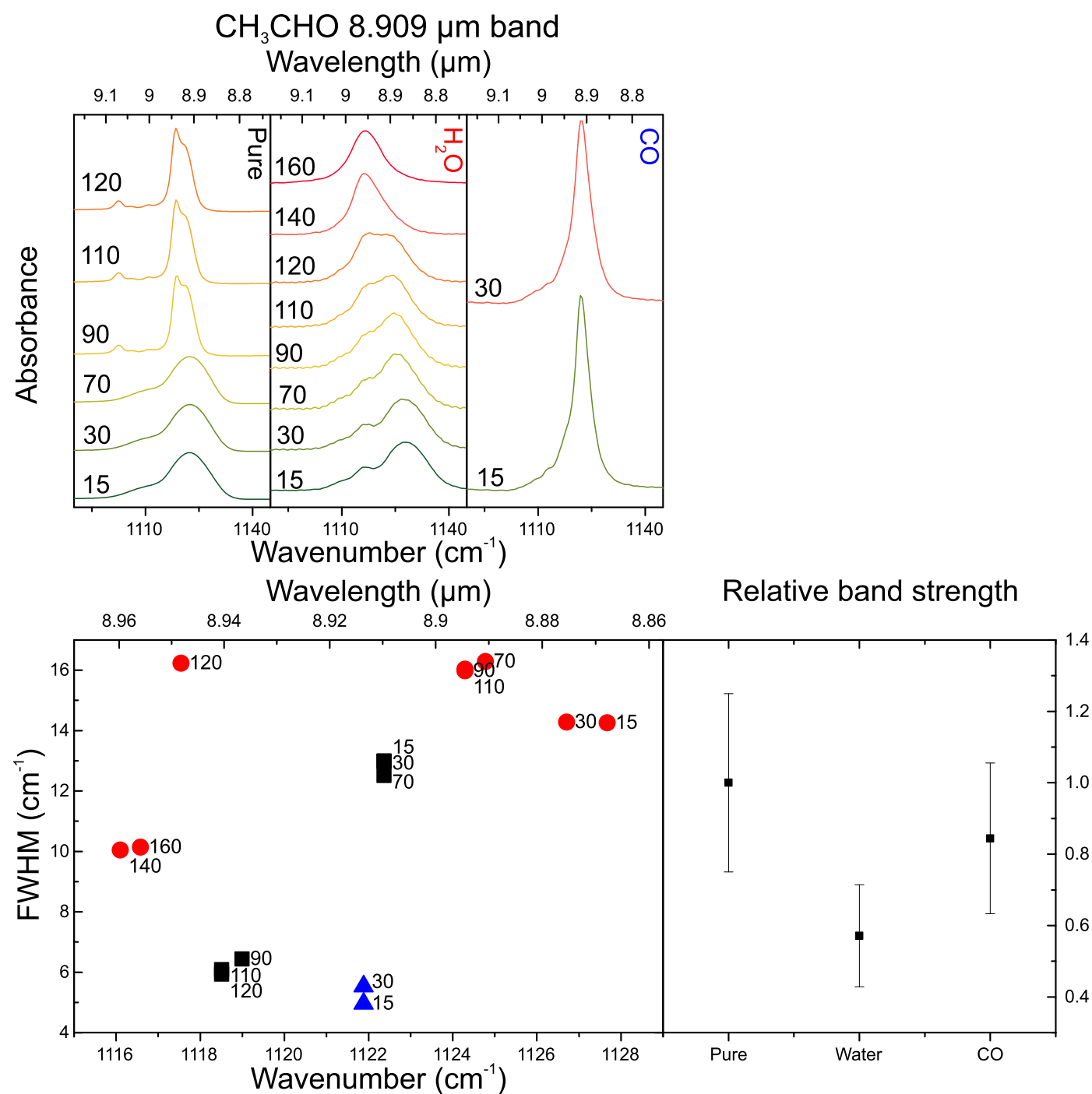
Fig. C.1. *Top*: *from left to right* the acetaldehyde 8.909 μm band pure (black) and in water (red) and CO (blue) at various temperatures. *Bottom left*: peak position vs. FWHM plot, using the same colour coding. *Bottom right*: the relative band strength for the 8.909 μm band at 15 K in various matrices.
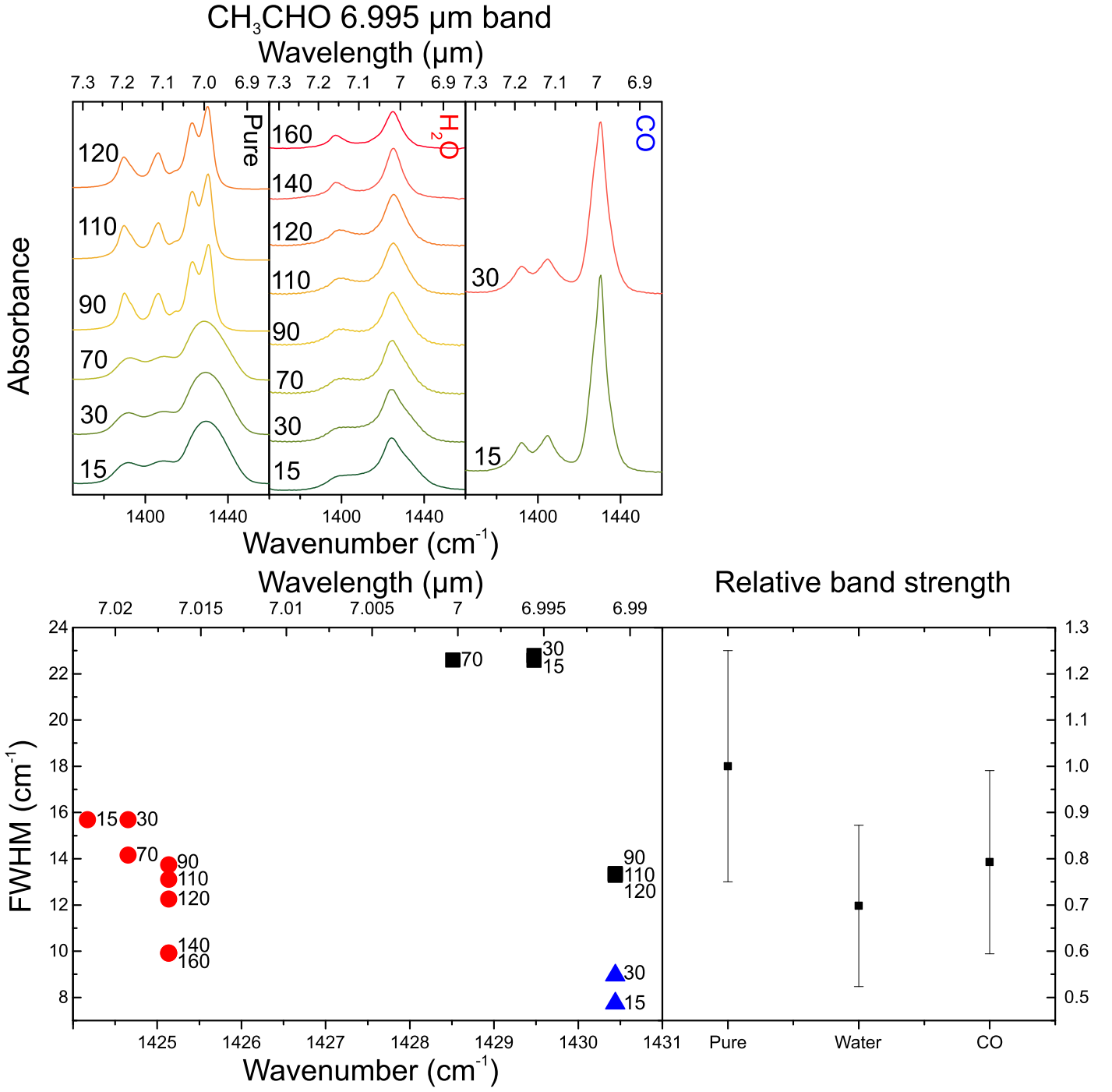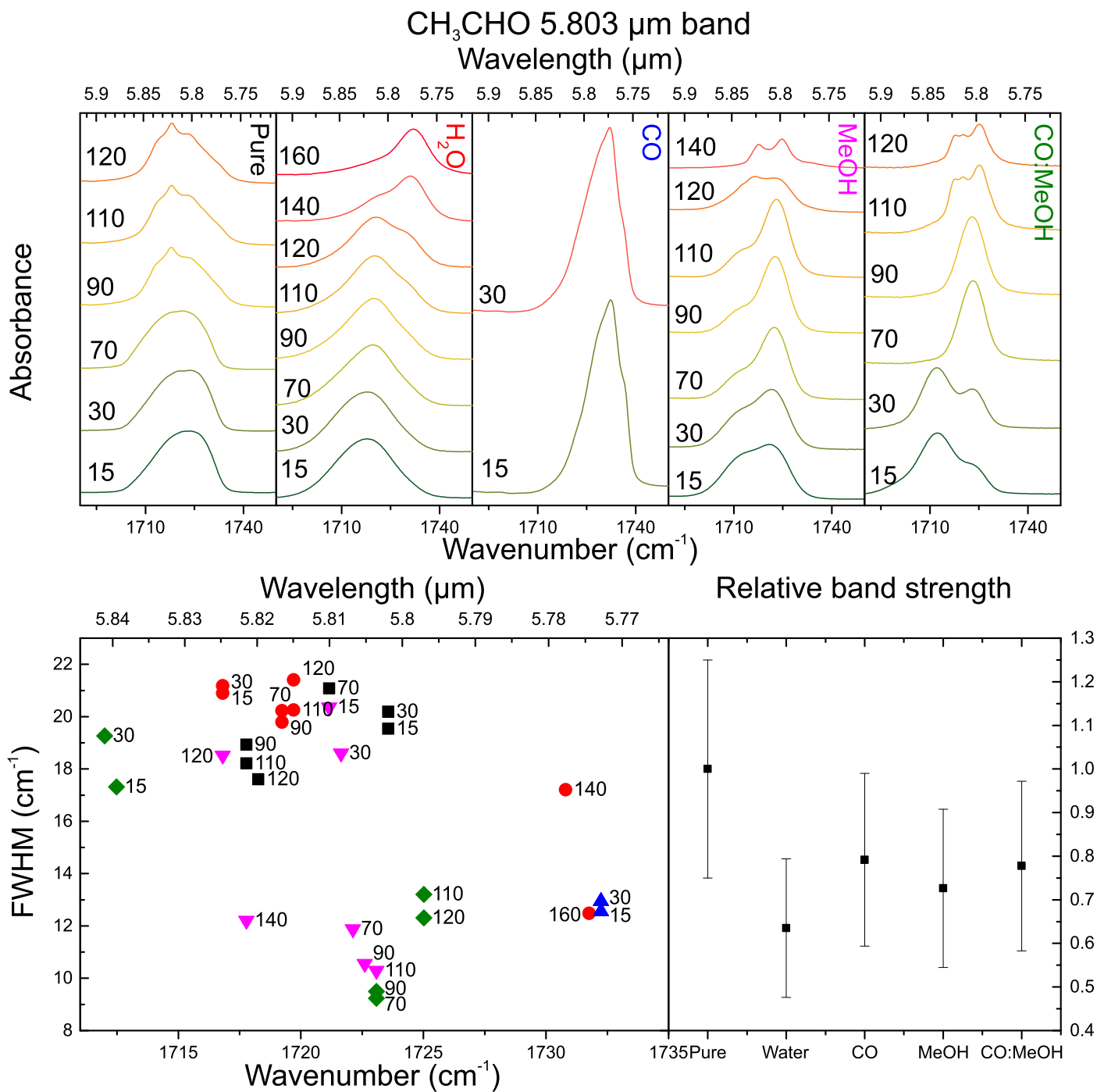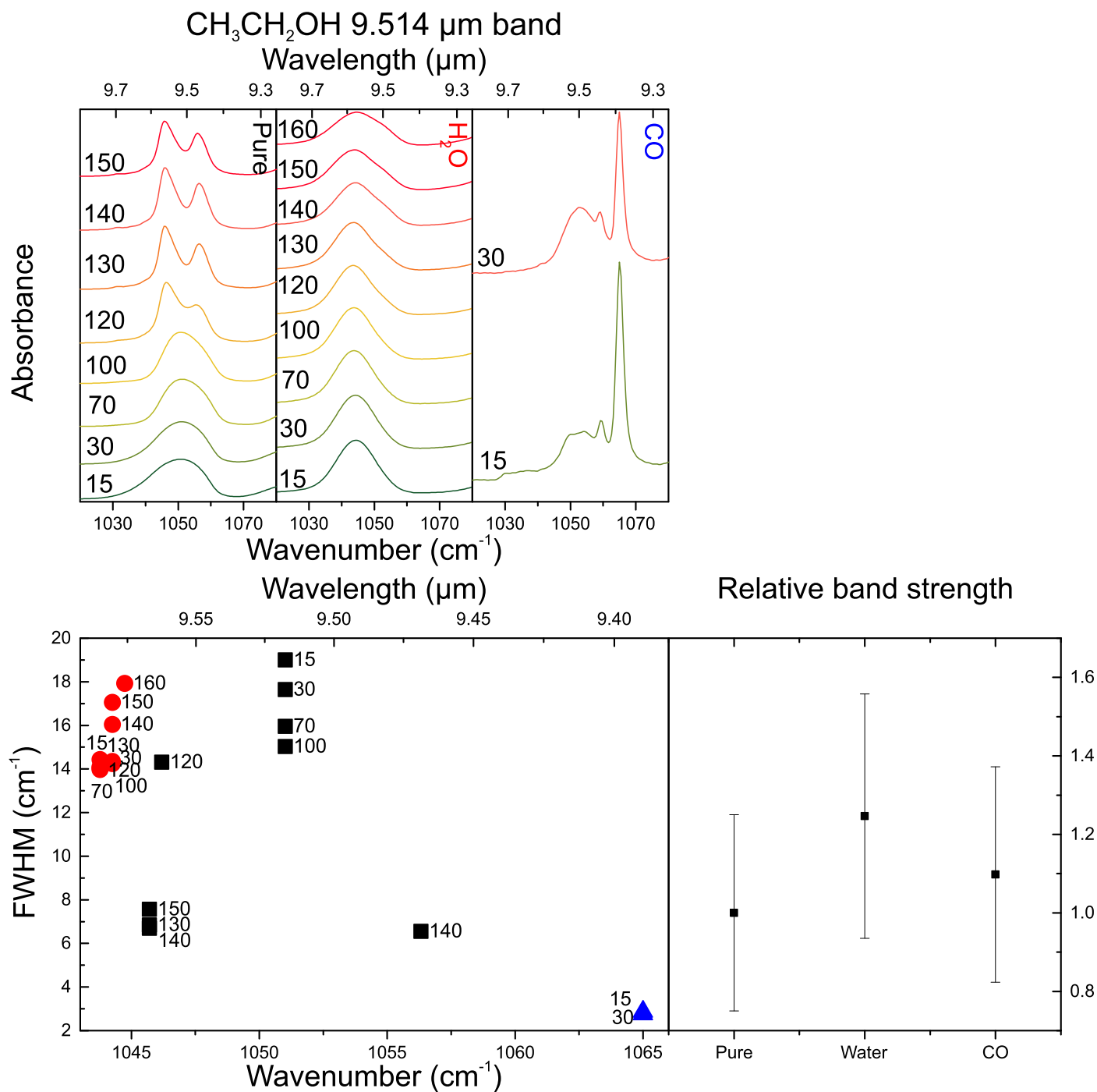
C.2. Ethanol

Fig. C.2. *Top*: *from left to right* the acetaldehyde 6.995 µm band pure (black) and in water (red) and CO (blue) at various temperatures. *Bottom left*: peak position vs. FWHM plot, using the same colour coding. *Bottom right*: the relative band strength for the 6.995 µm band at 15 K in various matrices.
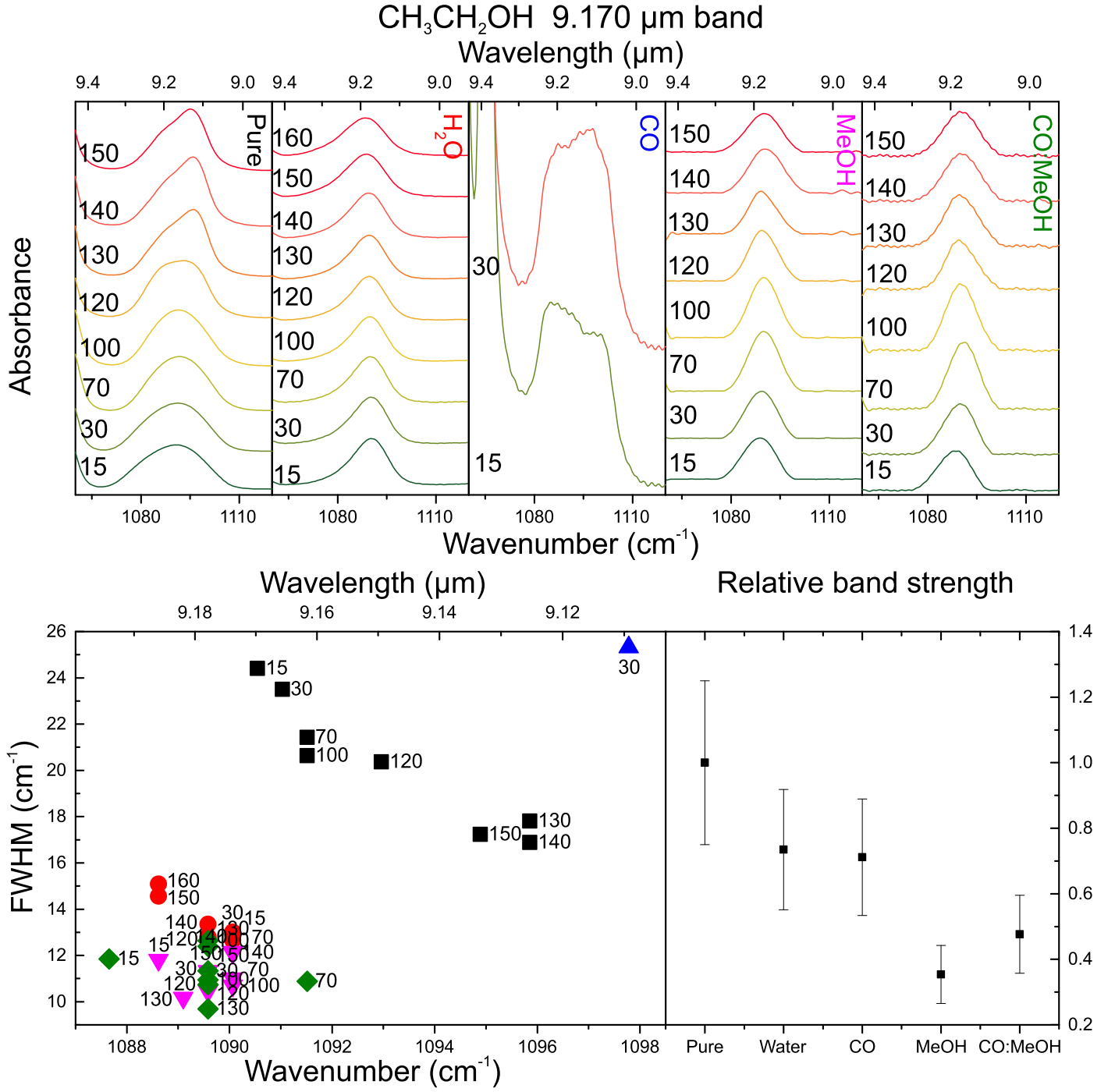
C.3. Dimethyl ether

Fig. C.3. *Top*: *from left to right* the acetaldehyde 5.803 μm band pure (black) and in water (red), CO (blue), methanol (purple), and CO:CH₃OH (green) at various temperatures. *Bottom left*: peak position vs. FWHM plot, using the same colour coding. *Bottom right*: the relative band strength for the 5.803 μm band at 15 K in various matrices.
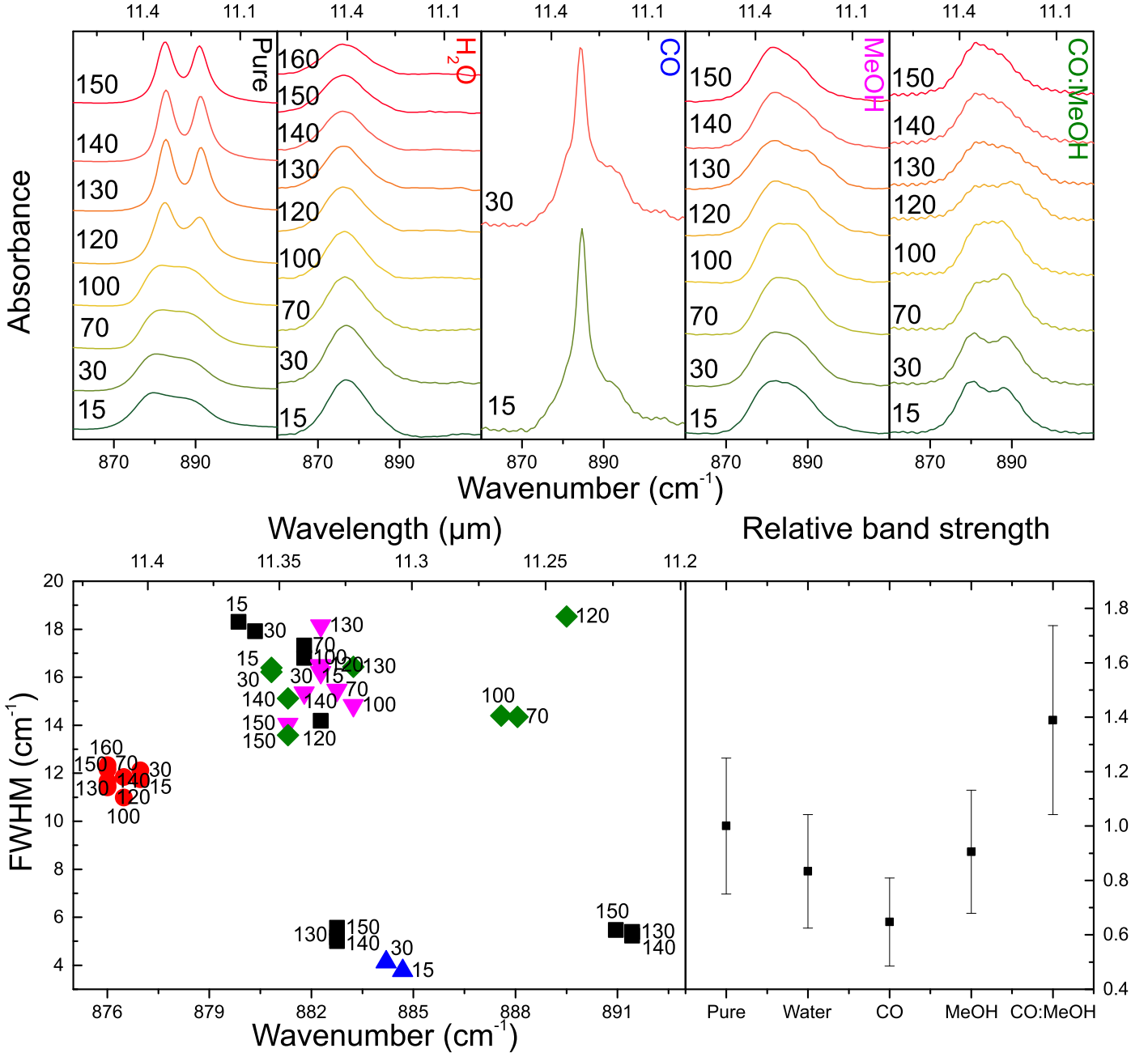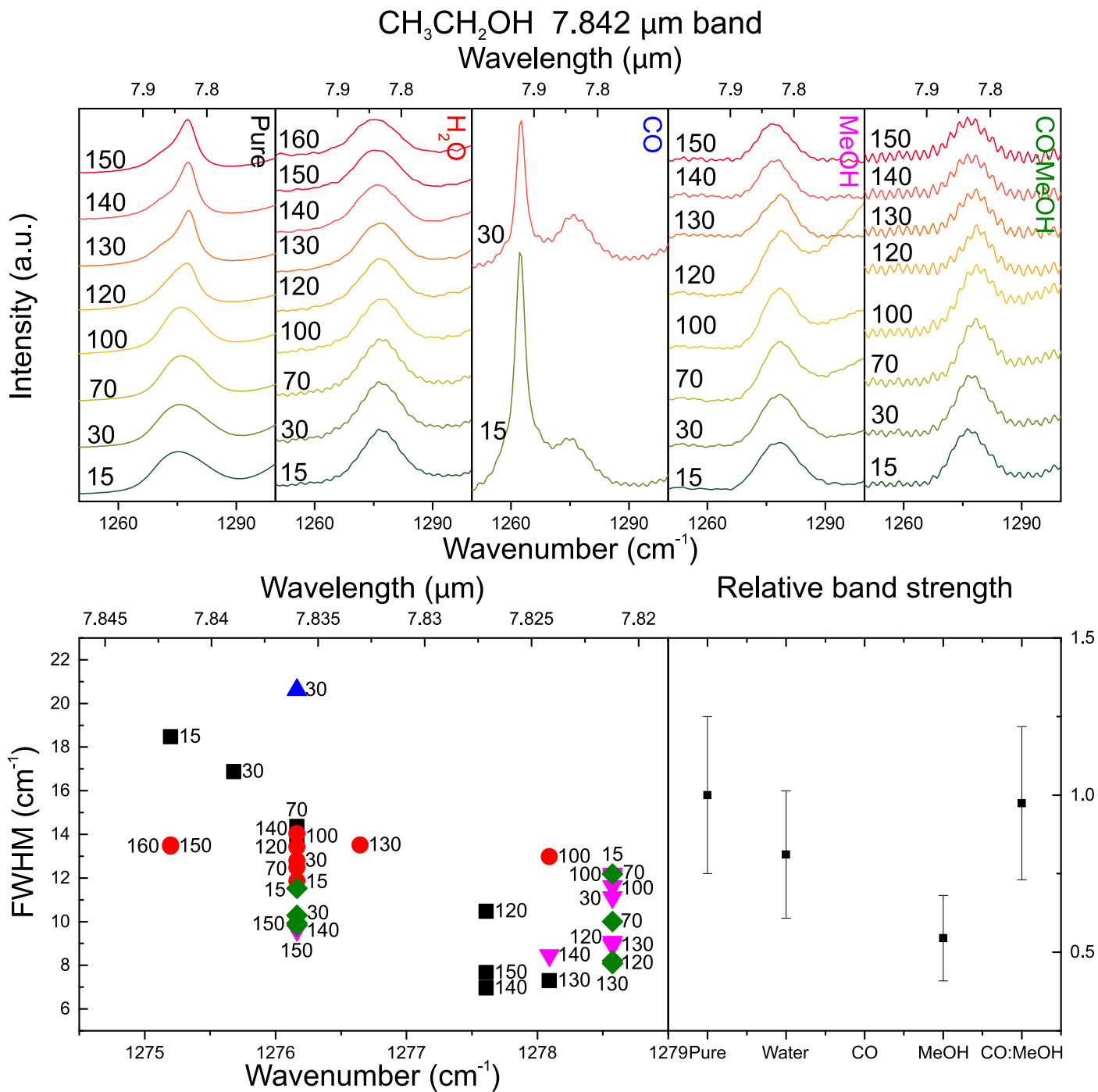
Fig. C.4. *Top*: *from left to right* the ethanol 11.36 μm band pure (black) and in water (red), CO (blue), methanol (purple), and CO:CH$_3$OH (green) at various temperatures. *Bottom left*: peak position vs. FWHM plot, using the same colour coding. *Bottom right*: the relative band strength for the 11.36 μm band at 15 K in various matrices.

Fig. C.5. *Top*: *from left to right* the ethanol 9.514 μm band pure (black) and in water (red) and CO (blue) at various temperatures. *Bottom left*: peak position vs. FWHM plot, using the same colour coding. *Bottom right*: the relative band strength for the 9.514 μm band at 15 K in various matrices.
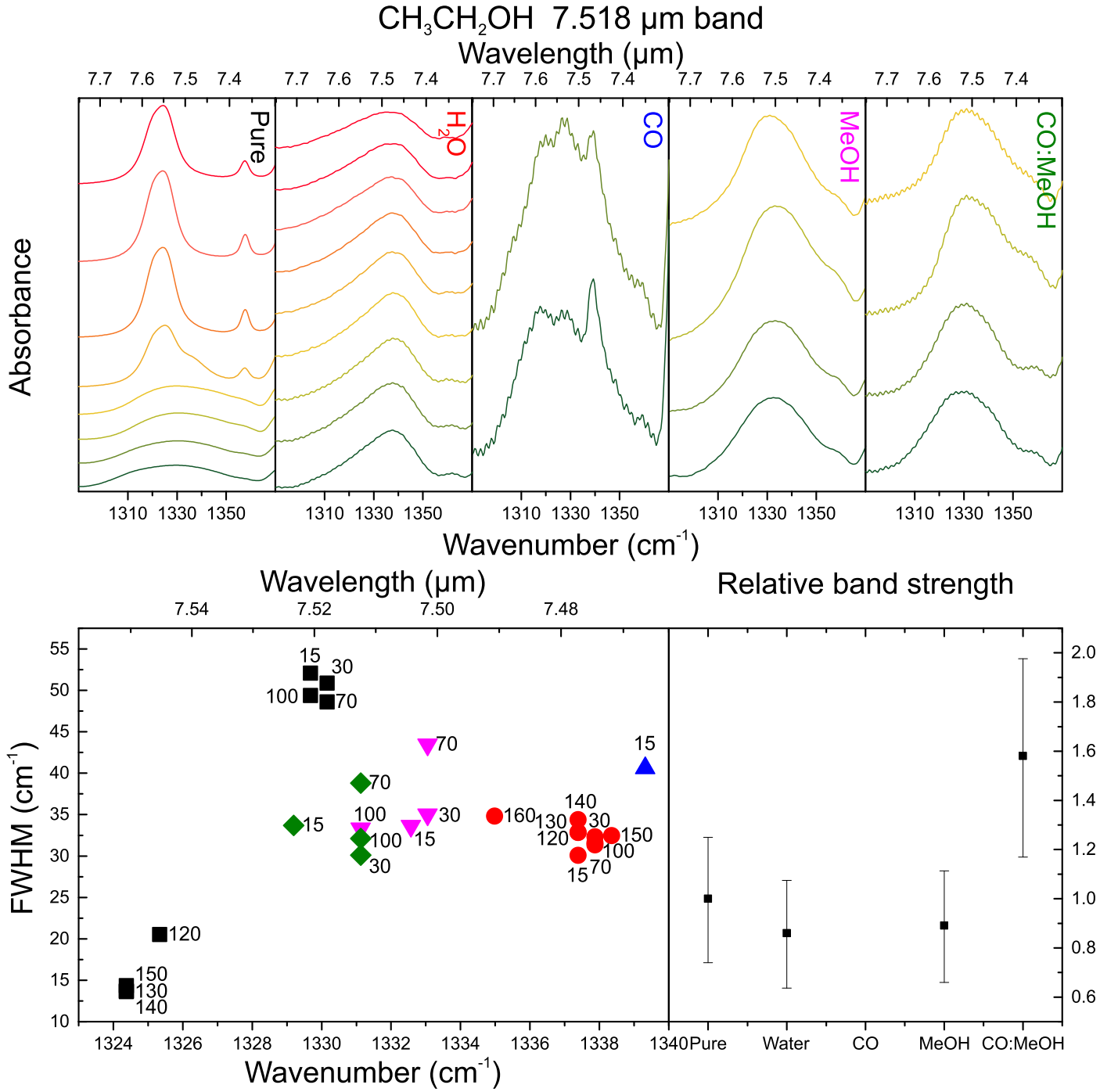
Fig. C.6. *Top*: *from left to right* the ethanol 9.170 µm band pure (black) and in water (red), CO (blue), methanol (purple), and CO:CH_3OH (green) at various temperatures. *Bottom left*: peak position vs. FWHM plot, using the same colour coding. *Bottom right*: the relative band strength for the 9.170 µm band at 15 K in various matrices.

Fig. C.7. *Top*: *from left to right* the ethanol 7.842 μm band pure (black) and in water (red), CO (blue), methanol (purple), and CO:CH₃OH (green) at various temperatures. *Bottom left*: peak position vs. FWHM plot, using the same colour coding. *Bottom right*: the relative band strength for the 7.842 μm band at 15 K in various matrices.
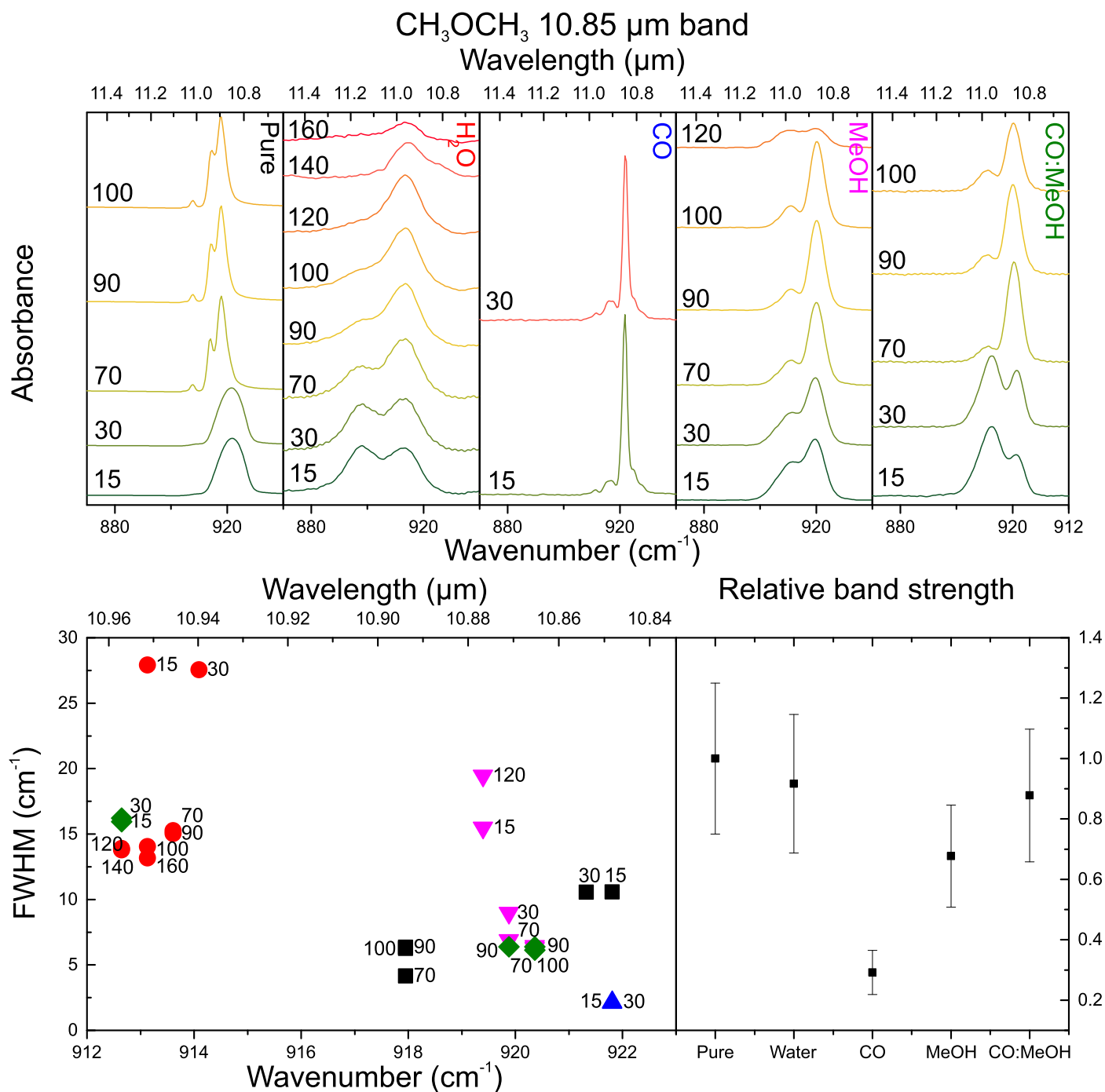
Fig. C.8. *Top*: *from left to right* the ethanol 7.518 μm band pure (black) and in water (red), CO (blue), methanol (purple), and CO:CH₃OH (green) at various temperatures. *Bottom left*: peak position vs. FWHM plot, using the same colour coding. *Bottom right*: the relative band strength for the 7.518 μm band at 15 K in various matrices.
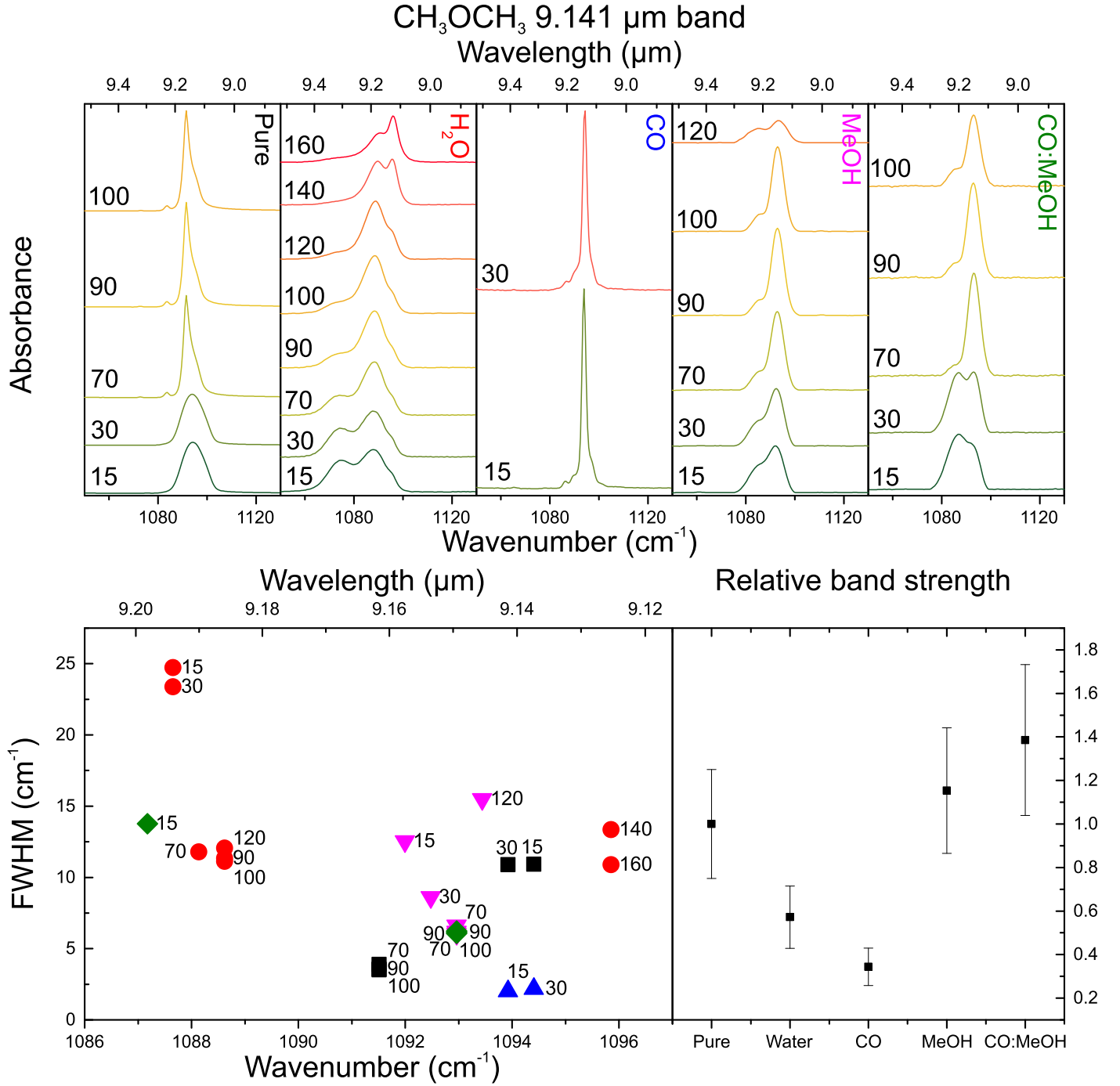
Fig. C.9. *Top*: *from left to right* the dimethyl ether 10.85 μm band pure (black) and in water (red), CO (blue), methanol (purple), and CO:CH₃OH (green) at various temperatures. *Bottom left*: peak position vs. FWHM plot, using the same colour coding. *Bottom right*: the relative band strength for the 10.85 μm band at 15 K in various matrices.

Fig. C.10. *Top*: *from left to right* the dimethyl ether 9.141 μm band pure (black) and in water (red), CO (blue), methanol (purple), and CO:CH$_3$OH (green) at various temperatures. *Bottom left*: peak position vs. FWHM plot, using the same colour coding. *Bottom right*: the relative band strength for the 9.141 μm band at 15 K in various matrices.
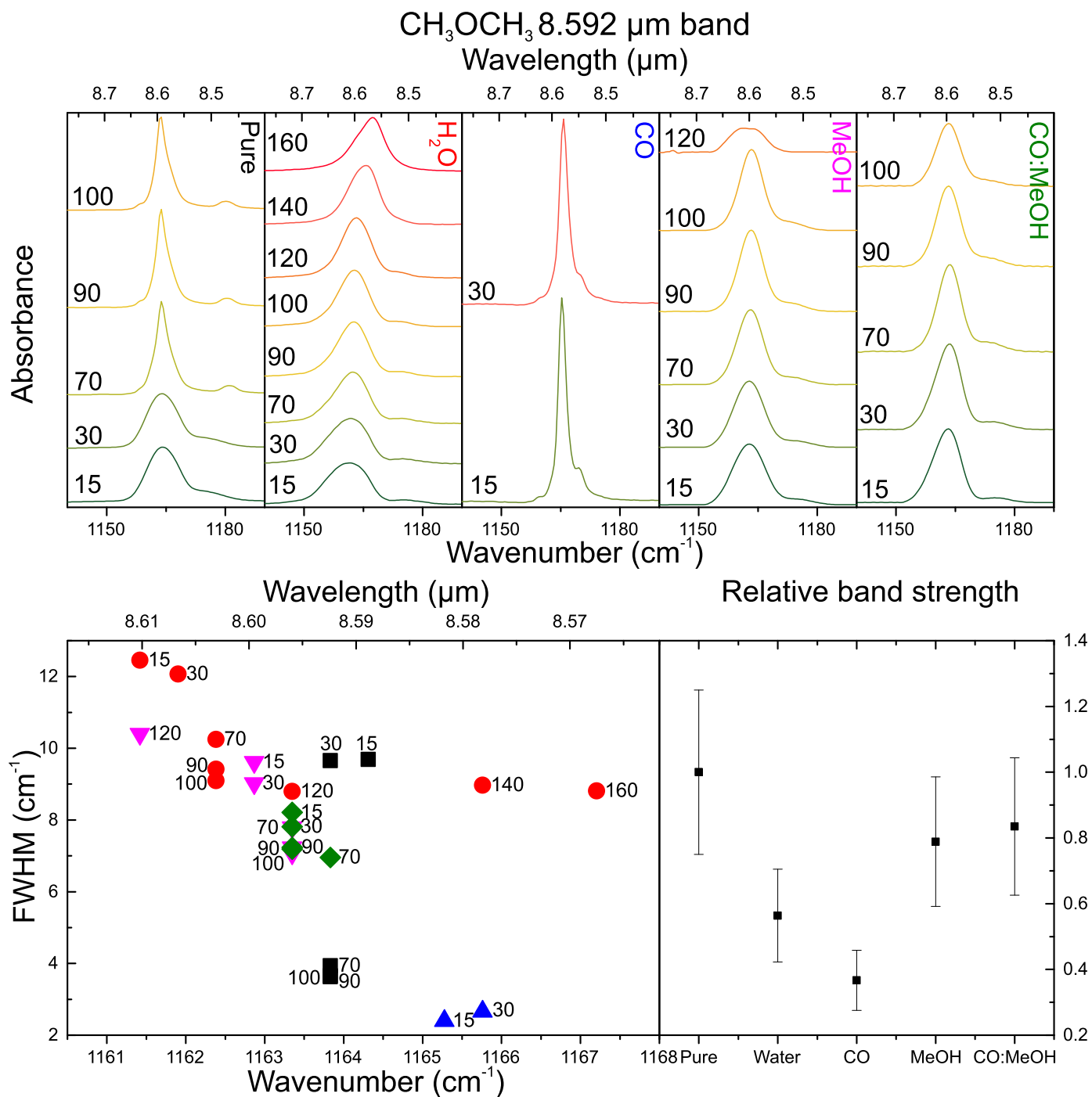
Fig. C.11. *Top*: *from left to right* the dimethyl ether 8.592 μm band pure (black) and in water (red), CO (blue), methanol (purple), and CO:CH₃OH (green) at various temperatures. *Bottom left*: peak position vs. FWHM plot, using the same colour coding. *Bottom right*: the relative band strength for the 8.592 μm band at 15 K in various matrices.